WAVE-PACKET CONTROL IN CYANINE DYES

By

Maryann Laboe

A THESIS

Submitted to
Michigan State University
in partial fulfillment of the requirements
for the degree of

Chemical Engineering – Master of Science

2021

ABSTRACT

WAVE-PACKET CONTROL IN CYANINE DYES

By

Maryann Laboe

Cyanine Dyes have a broad range of application because of their dual fluorescent properties. Still, there is much that is unknown regarding the excited state dynamics of these dyes, and even less known about their molecular dynamics in upper excited states. Chirp-manipulation, steady-state measurements, time-correlated single photon counting, kinetics modeling and theoretical calculations all aided in the understanding of differentiated linear and non-linear activated excited state relaxation pathways that led to altered S_2/S_1 dual fluorescence for both IR144 and IR140. Non-linear excitation takes place in response to the dual action of a high viscous environment and high photon density with decreased second order dispersion. This non-linear excitation is best understood as two-photon excitation. By altering viscosity and pulse chirp, linear and non-linear processes within the excited states of these molecules can be selectively controlled. It is observed that two-photon excitation elicits increased S_2/S_1 dual fluorescence ratios in both cyanine dyes and that this increase is maximized further in higher viscosity solvents. It is important to conclude that there is not only an increase in the S_2/S_1 fluorescence ratio with higher viscosity solvents, but there is a multiplicative effect, as chirp is manipulated.

I dedicate this thesis to my parents, Betsy and Kevin, who are always my biggest supporters. To my brother, Daniel, for keeping life interesting with his endless debates. To Bilbo Baggins, my large white dog, who consistently sits on top of me with his 90-pound self. And lastly, but most importantly, to God. My relationship with Him through Jesus is my greatest source of joy.

ACKNOWLEDGEMENTS

First, I would like to thank Michigan State University and the Department of Chemical Engineering and Material Science for their support during my time in graduate school. In addition, I'd like to thank the Department of Chemistry at Michigan State University. To everyone in the Dantus Research Lab, thank you for your comradery and for being a part of my time here at MSU, particularly Jurick, you have been a great help while I have been in the Dantus Research group. I would like to extend a special thank you my advisor, Dr. Marcos Dantus, for his support during this project and his guidance. To all the collaborators on this work, thank you. Dr. Ben Levine and Fangchun Liang, thank you for your theory expertise. Thank you to the Beck Research Lab for use of your lab and thank you Nila for all your time and assistance. Lastly, a big thank you to the National Science Foundation for funding my research under the grant CHE 1836498.

TABLE OF CONTENTS

LIST OF TABLES

LIST OF FIGURES

KEY TO ABBREVIATIONS AND SYMBOLS

CI	Conical Intersection
EEM	Excitation Emission Matrix
eV	electron Volts
FC	Frank Condon
fs	Femto-Seconds
IC	Internal Conversion
ICG	Indocyanine Green
IR	Infrared Radiation
IR144	2-[2-[3-[[1,3-dihydro-1,1-dimethyl-3-(3-sulfopropyl)-2H-benz[e]indol-2-ylidene]ethylidene]-2-[4-(ethoxycarbonyl)- 1-piperazinyl]-1-cyclopenten-1-yl]ethenyl]-1,1-dimethyl-3-(3-sulforpropyl)-1H-benz[e]indolium hydroxide, inner salt, compound with n,n-diethylethanamine
IR140	5-chloro-2-[2-[3-[(5-chloro-3-ethyl-2(3H)-benzothiazol- ylidene)ethylidene]-2-(diphenylamino)-1-cyclopenten- 1-yl]ethenyl]-3-ethyl benzothiazolium perchlorate
ISC	Intersystem Crossing
MIIPS	Multi-photon Intrapulse Interference Phase Scan
NC	Negative Chirp
PC	Positive Chirp
PS	Photosensitizer
S_1	First Singlet Excited State
S_2	Second Singlet Excited State
S_2^L	Lower Energy Second Singlet Excited State Minimum
S_2^H	Higher Energy Second Singlet Excited State Minimum

TCSPC	Time-correlated Single Photon Counting
TL	Transform-Limited
TPE	Two Photon Excitation
SLM	Spatial light modulator
υ	wavenumber
λ	wavelength
φ_2	chirp
f	4*ln(2)
τ_{in}	TL pulse duration (input pulse duration)
τ_{out}	pulse duration (output pulse duration)

INTRODUCTION

Molecular fluorescence is often used to describe the time-dependent dynamics that govern molecular relaxation from the initial excited state to the ground state. Before excitation, most molecules, in their ground state, have a singlet electron configuration. According to the selection rules within quantum mechanics, linear excitation of non-centrosymmetric molecules will result in a *gerade* transition, a singlet to singlet transition. Here, we focus on two non-centrosymmetric molecules. To excite a molecule, the energy of light used must equal the energy gap between the ground and excited state. Each molecule has a vibrational wave-function associated with each vibrational level within each excited energy state and its ground state. The transition moment integral calculates the probability of a transition by incorporating the wavefunctions of the two corresponding states as well as the transition dipole moment. The most probable state for the molecule to arrive at after excitation with a specific wavelength value is called the Frank Condon (FC) region. Upon excitation, the molecule reaches the FC region, while maintaining its ground state geometry. Relaxation from the FC region can be analyzed, and the relaxation pathways involved can appropriately be categorized as the molecule's wavepacket dynamics. More specifically, a wavepacket is a linear superposition of vibrational states in the excited state. After excitation, the wavepacket formed, far from equilibrium, flows down the multidimensional potential energy surfaces.

Upon excitation to the FC region, a molecule's wavepacket dynamics are regulated by competing relaxation rates associated with each location on the potential energy surface. Intersecting potential energy surfaces decrease the likelihood of fluorescence from the higher energy surface associated. These intersections are called conical intersections (CI). According to Kasha's rule, molecules excited to upper excited states will relax to the first excited state before

a considerable amount of fluorescence is observed.[1] Within the first excited state, as the non-radiative rates go up, the probability of fluorescence from the corresponding state goes down and vice versa. Internal conversion (IC) occurs as the molecule's wavepacket travels through a CI from one excited state to a lower excited state or to the ground state. This transition must occur between energy levels of the same multiplicity.

If the radiative rates are competitive with the non-radiative rates within a specific excited state, fluorescence is observed. As the radiative rate to non-radiative rate ratio increases, increased fluorescence can be observed. Increased solvent viscosity decreases the IC rate and thus increases fluorescence yield.[2,3,4] This is further analyzed with chirped pulse spectroscopic experiments on two cyanine dyes; IR144 and IR140.

Cyanine dyes are unique in that they emit fluorescence in measurable amounts from two excited states, exhibiting dual fluorescence, but the majority of their fluorescence yield is collected from their first excited state (S_1). Understanding the effects of the solvent and laser pulse shape on the optical excitation process leads to increased knowledge about wavepacket dynamics in cyanine dyes. The IC rate and excitation method play a large role in IR144 and IR140 wave-packet dynamics and relaxation pathway selection.

Dual fluorescence, more plainly articulated, is fluorescence from two different excited states after excitation to one excited state. This type of behavior violates Kasha's rule that, as stated above, molecules only fluoresce in considerable amounts from their lowest excited state. Beyond that, we show that the dual fluorescence ratio S_2/S_1 for IR144 and IR140 can be controlled by linear and non-linear excitation pathways and by varying solvent viscosity. Here, increasing solvent and viscosity and non-linear excitation increases the S_2/S_1 ratio, considerably. This work is important and instructive because it illustrates the effects that the paired process of

pulse chirp and viscosity have on molecular wavepacket dynamics in cyanine dyes. The ability to control the S_2/S_1 fluorescence ratios in these dyes could be applied to other cyanine dyes and even other fluorescent dyes. This is a valuable tool in processes aiming towards higher energy utilization, conserving energy or identifying and exploiting molecular environment.

CHAPTER 1: Background

Introduction

Cyanine dyes were first discovered in 1856 by Greville Williams.[5] They are versatile in application and thus an important molecule to study. They are characterized by an odd numbered conjugated π chain connecting two nitrogen rings, with a range of different types of side chain structures. Longer π chain systems between the two nitrogen rings require lower energy light to excite the molecule to S_1. Short chains, with only three to five carbons require ultraviolet (UV) or visible light to reach the first excited state, while dyes with seven carbons are considered infrared (IR) dyes. IR dyes have many medicinal applications because they use IR light for excitation, which falls within the therapeutic window.

In the case of biomolecular labeling, the side chains attached to each nitrogen can alter a cyanine dye's binding affinity. Charged side chains increase binding probability, while other side chain characteristics can alter its specificity for different types of molecules within a cell.[6] Side chain length has been shown to be of importance in cell permeability in other fluorescent molecules.[7] In addition, some cyanine dyes have substituents attached to the central carbon of their conjugated π chain. These substituents have been shown to play a role in ground state molecular conformation as well as molecular rotations in the excited state.[8]

Another important characteristic of cyanine dyes is that they emit phosphorescence, which is involved in triplet state radiative relaxation. Many cyanine dyes possess singlet excited states with CI's to triplet excited states. If a molecule moves through this intersection, it is called intersystem crossing (ISC). Since triplet states are usually lower in energy, the CI creates a likely avenue for the wave-packet to take as it relaxes to the ground state. Molecules with triplet

excited state yields can be referred to as photosensitizers (PS)'s. Molecules in their triplet state can react with molecular oxygen, resulting in free radical production. In vivo in cancer cells, molecular excitation of accumulated PS's results in cell death due to high levels of reactive oxygen species within the cell.[9,10]

Heptamethine Dyes

Since cyanine dyes are characterized by the number of methine carbons between their nitrogen atoms, those with seven conjugated π carbons are called heptamethine cyanine dyes. These dyes all fit within the therapeutic window, yet indocyanine green (ICG) is the only FDA approved heptamethine dye.[11]

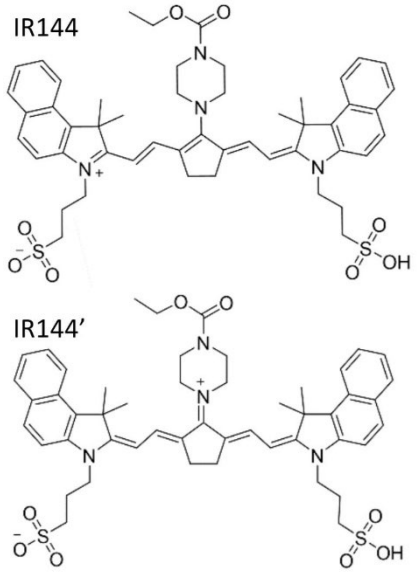

Figure 1.1: IR144 ground state conformations.

Several cyanine dyes have substituents attached to the central carbon of their π conjugated system. These substituents range from small alkyl groups to large ring structures.

Still others have the substituents attached by an amine group. This paper focuses on two heptamethine dyes in particular; IR144 and IR140, that differ mainly in their amine substituent.

IR144

IR144 is a heptamethine cyanine dye with a meso-amine substituent that is characterized by piperazine with ethyl acetate branching from its second nitrogen. It is a charged molecule with a dipole between the two charged groups. It has two conformations shown in the figure below that represent cyanine-like and bis-dipolar conformations for IR144 and IR144', respectively. The cyanine-like conformation has more flexibility around its amine substituent branch. Whereas the bis-dipolar conformation has less flexibility because it is attached to the heptamethine chain by a π bond. IR144 has a somewhat bulky amine substituent because of that may be more likely to have the cyanine-like conformation to allow rotation. The bis-dipolar conformation forms a parallel structure in which the amine substituent is in the same plane as the heptamethine chain.

IR140

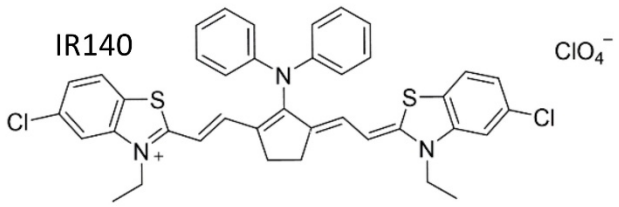

Figure 1.2: IR140's ground state conformation.

IR140 is a heptamethine dye with a bulky diphenylamino substituent. Its nitrogen atoms connecting the conjugated π system are part of a two-ring structure containing sulfur embedded,

with chlorine and an ethyl group branching from the nitrogen. Unlike IR144, IR140 only has one charge associate which gives it an overall positive charge. The associated perchlorate molecule together with IR140 create an overall neutral charge. IR140 has a cyanine-like configuration, but its bulky substituent creates steric hindrance causing less flexibility of its amine substituent.

CHAPTER 2: Experimental Methods

Introduction

To better understand IR144 and IR140 molecular dynamics in the excited state, the following experiments were conducted. Steady-state measurements in different viscosity solvents were performed to analyze the linear fluorescence and absorption spectrums and understand solvent effects. Time-correlated single photon counting (TSCPC) experiments were done to analyze the fluorescence lifetimes of S_2 and S_1 when the molecule is excited to the S_2 state. Solvent viscosity was varied within the TCSPC experiments to understand viscosity's effect on the time-component of these two excited states. MIIPS was utilized to introduce chirp to pulses on the femtosecond timescale. Fluorescence measured during these experiments offered information about the effect pulse duration has on the S_2/S_1 fluorescence ratio. In conjunction, power experiments were also conducted to further understand the influence photon density has on non-linear absorption.

Steady-State Spectroscopy

Serial dilutions of 50μM IR144 and IR140 were performed in methanol to find the optimal concentration. Here, the optimal concentration would be determined based off two competing effects: self-absorption and absorbance strength at the excitation wavelength. If the concentration is too high, self-absorption can shift peak fluorescence. On the other hand, if the concentration is too low, the absorption strength will go down.

For all the experiments, an excitation wavelength of 522 nm was used, and the corresponding fluorescence was collected. 522 nm excitation accesses the S_2 absorption band for both IR144 and IR140. Fig. 2.1 illustrates dual fluorescence from both the S_2 and S_1 excited states following S_2 excitation. The S_1 absorption band is also shown to have a peak around 740 nm for IR144 in glycerol (in Fig 2.1). For data analysis, the fluorescence underneath each curve was integrated with respect to wavenumber. A more detailed explanation of these calculations is located in the "MIIPS Chirp Experiment" section.

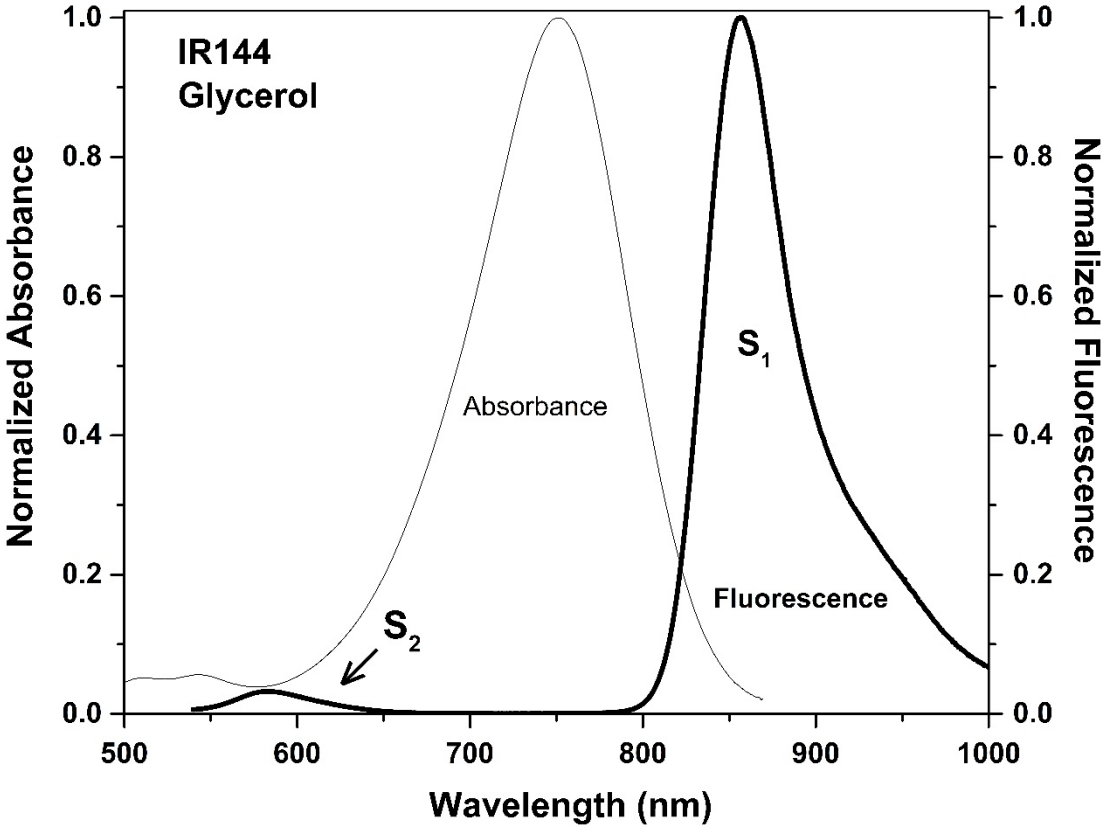

Figure 2.1: 50uM IR144 in glycerol absorbance (thin line) and fluorescence (thick line) spectra with respect to wavelength. Dual fluorescence is displayed from S_2 and S_1 excited states, following 522 nm excitation.

IR144 and IR140 were placed in quartz cuvettes so that UV light would have access to the sample. Absorption spectra were taken at each of these concentrations (50, 25, 16.7, 12.5, 6.25, 3.125 & 1.56μM) with identical spectra. S_1 peaks were around 0.3 at 16.7μM for both IR144 and IR140, but S_2 peaks only reached 3% of the S_1 maxima, therefore at 16.7μM, the absorbance values for S_2 were around 0.009. After excitation, fluorescence was measured at 50μM and at subsequent serial dilutions from 50μM (25, 12.5, 6.25, 3.125 & 1.56μM). It was found that S_1 fluorescence maximums shifted hypso-chromatically, to higher frequency values, as the concentration was decreased. This is indicative of self-absorbance and was confirmed by overlaying the fluorescence and absorption spectra.

This experiment focused on S_2 excitation, therefore although self-absorbance should be kept at a minimum, the molecule needs to be at a concentration conducive to absorbance at the excitation wavelength. S_1 fluorescence peak shifts came to a halt between 3.125 and 1.56μM, but this concentration range proved to be too low for exciting a measurable amount of molecules to be analyzed during our experiments. Taking into account both low S_2 absorbance and self-absorption, we concluded that there is not an optimal concentration for these experiments. Due to the high importance in determining fluorescence fluctuations in response to chirp, we deduced that a stable consistent signal was important, therefore 50μM was selected for each molecule.

50μM solutions of IR144 and IR140 were prepared in methanol, ethanol, n-propanol, ethylene glycol and glycerol. All solvents were purchased with spectrophotometric grade purity. Methanol, ethanol and n-propanol were kept in an airtight container and withdrawn using argon gas. Solutions were kept for a maximum of one week and were not used in experiments beyond that timeframe.

Absorption and fluorescence spectra were collected and recorded for each of the 10 samples. The transition dipole moment representation was implemented for both spectra. The absorption dipole strength is the absorption value divided by its wavenumber $A(\upsilon)/\upsilon$ and the fluorescence dipole strength was calculated by dividing the fluorescence values by their wavenumber cubed $F(\upsilon)/\upsilon^3$.

Excitation-emission matrix (EEM) spectra were also collected and recorded for IR144 and IR140 in methanol, n-propanol and glycerol. N-propanol is plotted in the results chapter. This experiment was conducted in our Horiba spectrometer. Excitation ranged from 250 to 900 nm in increments of 5 nm, while emission was collected at 1 nm resolution from 400 to 1100 nm. The EEM method excites the sample at a specific wavelength and probes for fluorescence at specific wavelength values, it then repeats this process for each selected excitation wavelength.

TCSPC Experiments

Time-correlated single photon counting was conducted for both IR144 and IR140 in methanol, ethylene glycol and glycerol. The samples were all excited with 531 nm light to the S_2 state by picosecond laser with a high repetition rate at 80 MHz. S_2 and S_1 decay were both collected at a 12.5 nm bandwidth with a central wavelength at their maximum values. With picosecond resolution, fluorescence decay times were collected for S_2 for both cyanine dyes in these three solvents. A filter was used to select for different wavelengths, so that the photomultiplier (PMT) that collected the signal would only detect signal from the selected wavelength range. Following the S_2 experiment, a new filter system was used to select for the S_1

maximum. Since the molecule was being excited to S_2, a rise and decay was observed for S_1 fluorescence as the S_1 excited state became populated from the S_2 state.

MIIPS Chirp Experiments

The multi-photon intrapulse interference phase scan (MIIPS) program[12,13,14] was implemented to generate ultra-short transform limited (TL) pulses from a femtosecond laser beam. The MIIPS pulse shaper has gratings that reflect each wavelength value in such a way that the phase of each frequency can be shifted. Different iterations of phase masks are placed on the pulses and the pulse duration, fidelity, time bandwidth product and central wavelength are recorded. The pulses were compressed to 19 fs with a central wavelength of 522 nm. The fidelity is a measure of comparison from pulse to pulse, we want to get as close to 1.0 as possible to ensure pulse precision.[14] The TBP measures the temporal and spatial components of the pulse and is important because it indicates how close a pulse is to TL. The TBP for a TL laser pulse is equal to the full width half max (FWHM) of a gaussian shaped pulse, around 0.44. We aimed to get as close as possible to that value.

To carry out this experiment, 50μM of IR144 and IR140 in methanol, ethanol, n-propanol, ethylene glycol and glycerol were prepared and placed in quartz cuvettes. The preparation specifics are identical to those indicated in the steady-state experimental methods above. The quartz walls were gently cleaned with methanol on all sides before being placed into the set-up.

Within the set-up, following the biophotonic solutions femoJock P pulse shaper, was a series of mirrors, followed by an internal attenuator inside the pulse shaper as well as an external

attenuator near the end of the beam path before the sample. The femtoJock P pulse shaper has one 128 pixel spatial light modulator (SLM), which limited the range of chirp that could be applied to the pulses. A focusing lens was placed in front of the sample and a cuvette holder held the quartz cuvette in place. The beam focused on the front corner of the inside of the cuvette to keep non-linearities at a minimum and allow for accurate collection of fluorescence perpendicular to the excitation beam. A very basic outline of the set-up is shown in figure 2.2 below.

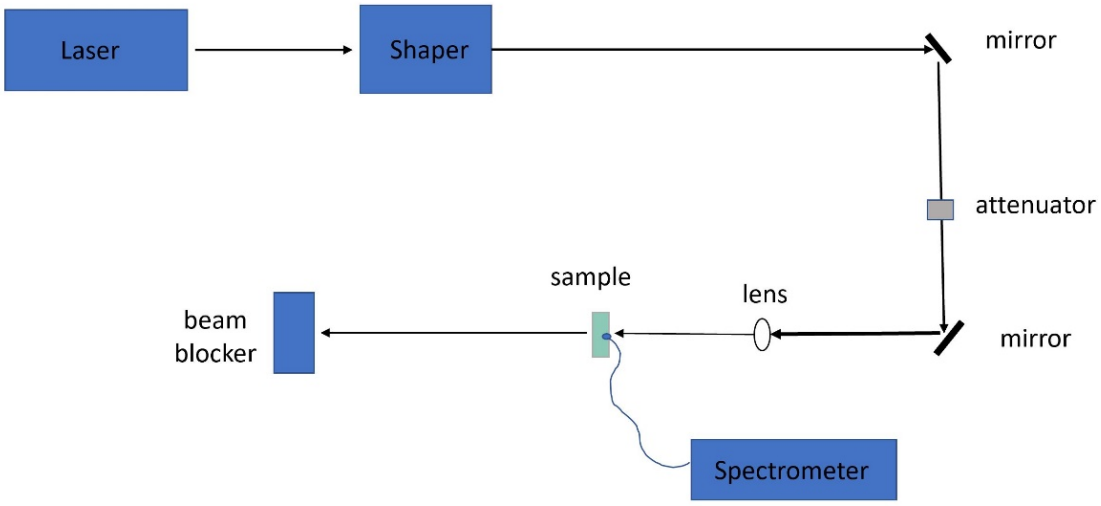

Figure 2.2: Experimental set-up for laser chirp experiments.

Before placing the samples in the beam path, an SHG crystal was put in place of the sample to measure SHG at differing chirp values. This was done to verify that the excitation pulse is hitting the sample with the correct phases applied. The MIIPS program corrects the pulse to TL using an SHG crystal and measuring the SHG of the laser beam. SHG is dependent upon photon density with no dependence on intra-pulse frequency ordering, meaning a symmetrical chirp scan would be produced with no differences between positive and negative chirp. MIIPS

determines which frequencies need to be phase-shifted to generate a TL pulse by measuring the outcoming photon intensity and spectrum. A quartz slide with a thickness equal to the cuvette wall was placed in the beam path to correct for dispersion introduced by the cuvette wall.

Once the MIIPS program compresses the pulses to TL, experimentation can begin. Chirp (second order dispersion) was applied to the pulses by way of chirp scans. Chirp values ranging from -15,000 fs^2 to +15,000 fs^2 were applied to the pulses with 300 fs^2 step sizes. At each chirp value, the resulting fluorescence spectrum was measured and averaged. At least three to five scans were done for each sample.

During these experiments it was observed that IR144 and IR140 have a high sensitivity to different laser power values. As power intensity increased, not only did the overall fluorescence yield go up, but the S_2/S_1 ratio went up. Therefore, power dependent experiments were conducted to further understand this phenomenon. These experiments are explained in the "power-dependence" section.

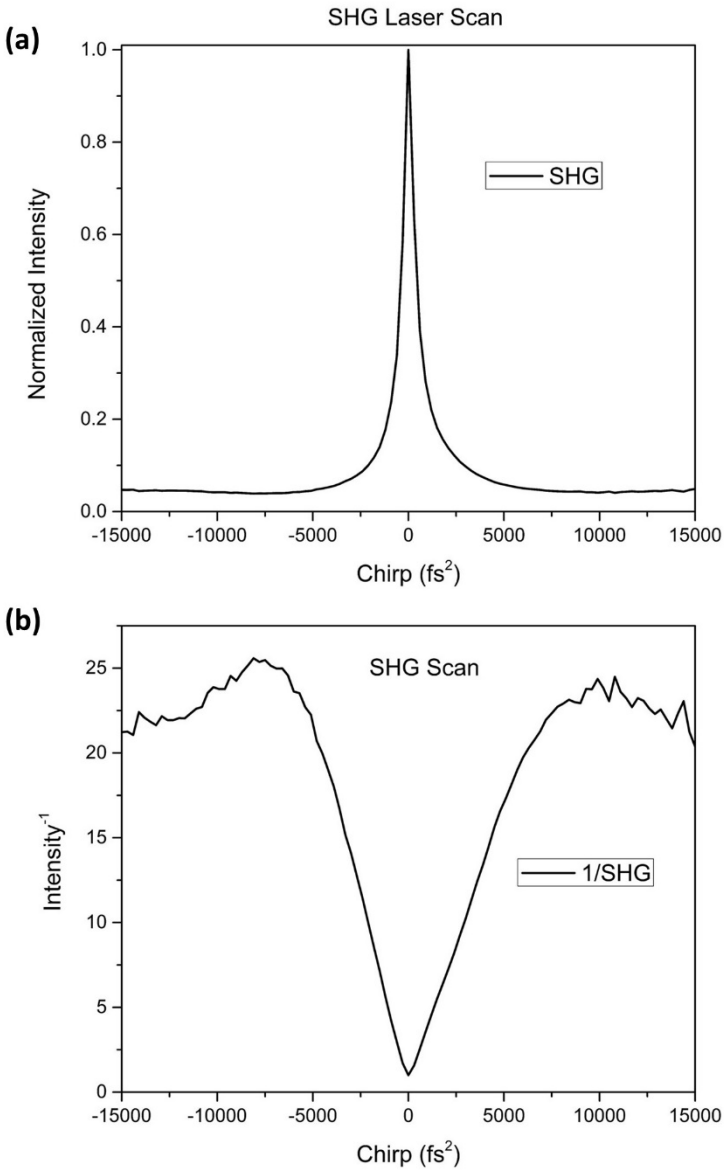

Figure 2.3: Laser light with a central wavelength of around 261 nm was collected after 522 nm laser light was focused on an SHG crystal. (a) SHG generation as a function of chirp and (b) the inverse of normalized SHG as a function of chirp are plotted.

SHG and laser scans were collected at the chirp range used for our experiment. The SHG scan is shown in figure 2.3a and 1/SHG is in figure 2.3b. Before plotting 1/SHG, the SHG graph was normalized to a maximum value of 1. The magnitude of the slope of 1/SHG is indicative of the TL pulse duration before chirp is applied and should not change throughout the chirp scans.

In figure 2.3, beyond +/- 5,000 fs^2, chirp is no longer being applied in a linear fashion. Therefore, only values from +/- 5,000 fs^2 are included in the final experimental data. Within the data, each value along the 1/SHG line was used to calculate the actual chirp applied to the pulse at the specific point. The data was corrected using this method and the equations below. Equation 1 relates the TL pulse duration τ_{in} to the new pulse duration τ_{out} as different chirp values φ_2 are applied to the pulse. f is a constant used for Gaussian pulses, 4*ln(2).

$$\tau_{out} = \tau_{in}\sqrt{1 + f^2\left(\frac{\varphi_2}{\tau_{in}^2}\right)^2} \tag{1}$$

Equation 2 explains the inverse relationship between SHG and pulse duration as a function of chirp. This is intuitive since SHG is dependent on photon density.

$$SHG \propto \frac{\tau_{out}}{\tau_{in}} = \frac{1}{\sqrt{1 + f^2\left(\frac{\varphi_2}{\tau_{in}^2}\right)^2}} \tag{2}$$

τ_{out} changes with respect to φ_2 and the slope is $(1/\tau_{in})$. Taking a constant input pulse of 20 and a chirp range of +15,000 fs^2 to -15,000 fs^2, a 1/SHG graph is simulated below in figure 2.4.

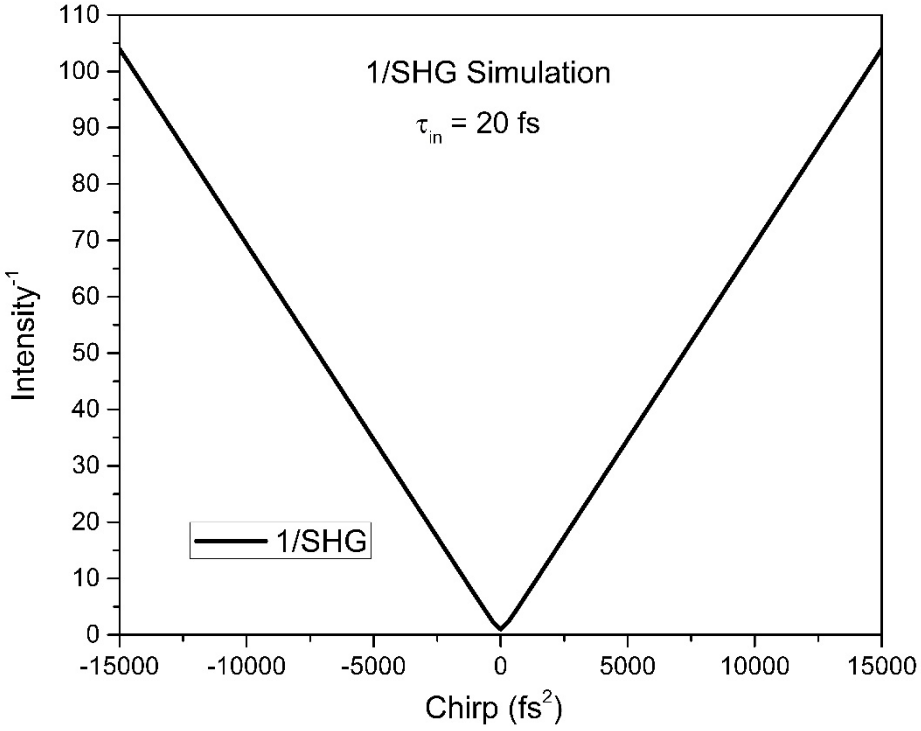

Figure 2.4: An inverse SHG simulation with respect to chirp.

Figure 2.4 illustrates that the slope is linear. From this slope, the expected φ_2 value can be calculated, shown in equation 3. This equation was applied to the experimental data to determine the actual chirp value at each data point.

$$\varphi_2 = \frac{\tau_{in}^2}{f}\sqrt{\left(\frac{\tau_{out}}{\tau_{in}}\right)^2 - 1} \tag{3}$$

Once the data was corrected and within the proper range, the zero-chirp value (TL) was more closely analyzed. For each chirp value, a fluorescence spectrum was collected. Each spectrum was transformed from fluorescence intensity with respect to wavelength to its transition dipole moment representation after being corrected for wavenumber. This transformation is shown in equation 4 and 5.

$$F(\nu) = F(\lambda) \times \lambda^2 \rightarrow \frac{F(\nu)}{\nu^3} \tag{4}$$

$F(\nu)/\nu^3$ represents the fluorescent dipole strength. These values were then integrated with respect to wavenumber for the S_2 and S_1 spectral peaks. Integrated fluorescence values for both S_2 and S_1 were used as a reference and the changes were reported for each chirp value. The resulting values were calculated using equation 5.

$$\frac{(I - I_{TL})}{I_{TL}} \tag{5}$$

This was completed for each of the two energy states S_2 and S_1. I represents the integrated fluorescence dipole strength and I_{TL} represents the integrated fluorescence dipole strength at TL.

A graphical representation of this with respect to chirp was generated. We discovered that the TL pulses were mis-aligned by a chirp value of less than 300 fs^2. Since data points were only collected for every 300 fs^2, interpolated data points needed to be generated for an accurate shift. The curves in the graph represented a Lorentzian line-shape. Interestingly enough, the inverse of equation one, similar to equation 2 can be used to represent the S_2 line-shape. Once the curves were fitted, new data points could be both interpolated and extrapolated for accurate peak smoothing and representation of TL. Equation 6 below was used to fit the curves.

$$y = b + \frac{h}{\sqrt{1 + f^2\left(\frac{\varphi_2}{\tau_c^2}\right)^2}} \tag{6}$$

b, h and τ_c stand for baseline value, peak height and τ_{in}, respectively. τ_{in} is directly related to curve width and a width comparison was recorded for different solvents.

Power-Dependence Experiments

Due to an observed sensitivity of these cyanine dyes to laser power, a chirp experiment was run with IR144 and IR140 in methanol at different laser power values. Fluorescence spectra were collected at 300 fs^2 increments from -15,000 fs^2 to +15,000 fs^2. SHG experiments were also conducted and averaged in order to represent the chirp data accurately.

In addition, the S_2 spectra were more closely analyzed for positive chirp, TL and negative chirp values. Figure 1 illustrates that past +/- 5,000 fs^2, the SHG intensity is equal to chirp values ranging from +/- 4,000 – 5,000 fs^2. These values were used in addition to the actual +/- 4,000 – 5,000 fs^2 and averaged to report the average spectra for positive and negative chirp, respectively. All spectra were converted to their transition dipole moment representation before being presented graphically.

Power-dependent experiments were also conducted for IR144 and IR140 in ethanol, n-propanol, ethylene glycol and glycerol. The observed S_2/S_1 increase occurred at TL for high powers in lower viscosity solvents, but as viscosity increased high powers resulted in saturation. The S_2/S_1 increase was characterized by an increase in S_2 with a simultaneous decrease in S_1. This ratio was measured by integrating the fluorescence spectrum at each chirp value. Glycerol and ethylene glycol required powers at least 10-fold lower than the other solvents. The effects were only noticed within a small power range of around 0.25 mW. This is due to slow molecular movement out of the FC region in viscous solvents, which causes the samples to easily saturate.

Summary

The above experiments; steady state absorption, fluorescence and 2D EEM, TCSPC, chirp experiments, and power dependence experiments, along with theoretical and kinetic

calculations together were utilized to draw conclusions about the excited state dynamics of both IR144 and IR140. Steady-state data was utilized to understand the effects of solvent viscosity on linear absorption. TCSPC measurements verified solvent effects on fluorescence lifetimes for both S_2 and S_1. Chirp experiments brought a variety of information, from photon density to frequency dependence, to an ultrafast time-sensitive understanding of the excited state molecular dynamics. Power-dependence experiments aided the chirp experiments in further analyzing the importance of photon density. Finally, theory and kinetic calculations were carried out to make sense of our observations.

CHAPTER 3: Linear and Nonlinear Optical Processes Controlling S_2 and S_1 Dual Fluorescence in Cyanine Dyes

Introduction

Research Goal/Abstract

We report on the changes in the dual fluorescence of two cyanine dyes IR144 and IR140 as a function of viscosity and probe their internal conversion dynamics from S2 to S1 via their dependence on femtosecond laser pulse chirp.[15] Steady state and time-resolved measurements were performed in methanol, ethanol, propanol, ethylene glycol and glycerol solutions. Electronic structure calculations identified three low-lying excited states responsible for the experimental observations, S1, S1.5, and S2 State S1.5 was found to relax to the S1 minimum but the previously identified S2 state was found to relax to wo differently twisted minima. Chirp dependence measurements, aided by numerical simulations, provided dynamic clues regarding the internal conversion dynamics from S2 to S1 and its dependence on solvent viscosity and pulse duration. By controlling solvent viscosity, and pulse duration, we were able to control the S2/S1 population ratio of a factor of 86 and 55 for IR144 and IR140, respectively. The increase in the S2/S1 ratio is explained by a two-photon transition from S2 to an even higher excited state. The ability to maximize the population of higher excited states prior to non-radiative relaxation may lead to increased efficiency of photochemical processes.

Introduction

Fluorescence from high lying excited states is uncommon for organic molecules in solution because of the fast internal conversion (IC) to the lowest excited state of the same parity that gives rise to Kasha's rule.1 Here, we revisit the dual fluorescence observed in cyanine dyes,2,3,4 in particular, the enhanced S2 emission observed in studies using chirped femtosecond laser pulses.5 Here, we endeavor to understand what leads to the unusual enhancement by restricting molecular motion via changes in solvent viscosity and shaping the laser pulses. The motivation of our work is to learn how to enable new applications of cyanine dyes through increasing the lifetime of high lying excited states.

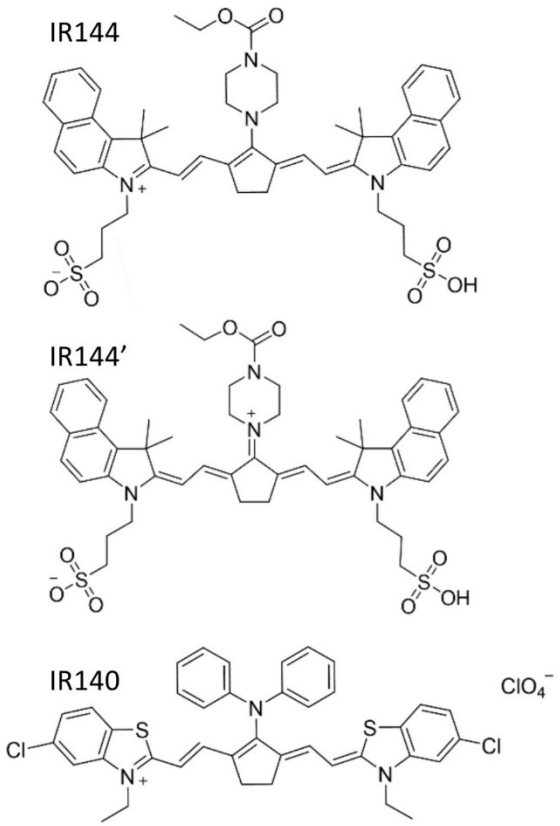

Figure 3.1: IR144 and IR144' represent two commonly understood conformations of IR144. IR140 mainly forms a cyanine-like conformation.

Cyanine dyes encompass a large category of fluorescence molecules with an odd numbered conjugated π-bonding system connecting two nitrogen atoms that branch off into a range of different substituents. Cyanine dyes are used in a wide range of applications, including bioimaging, [16,17,18,19,20] solar energy conversion,[8,21,22] photodynamic cancer therapy,[23,24] and textiles.[25] Their spectroscopic properties are easily tuned making them useful model compounds.[26] Here we focus on heptamethine cyanine dyes IR144 and IR140, shown in Figure 1, which differ in their amine substituent located in the center of their polymethine chain. IR144 has a piperazine substituent, while IR140 has a bulky diphenylamino group. The bulky substituent gives IR140 a higher degree of steric hindrance than IR144. Notice the two configurations for IR144 and IR144' represent the bis-polar conformation of IR144, while IR140 represented in the cyanine-like conformation.[21]

Here we use femtosecond chirped pulses to not only control photon density, but also to understand the time-correlated wave-packet motion that leads to IC. When an otherwise transform limited (TL) pulse is chirped, its pulse duration broadens. Therefore, chirp can be used to control the peak intensity of the pulses. More importantly, the instantaneous frequency sweeps from higher to lower frequencies in a pulse with positive chirp or from lower to higher frequencies in a pulse with negative chirp. The fast sweep in frequency can be thought of as using a pair of pulses with different frequencies separated by a time delay that is proportional to the chirp magnitude, and this makes chirp pulses useful for following molecular dynamics.[27,28,29,30,31,32] The 'chirp effect' following S_1 excitation consists of a decreased fluorescence yield observed for negatively chirped pulses compared to positively chirped pulses. This difference occurs because negatively chirped pulses are able to stimulate emission from the excited state, resulting in lower fluorescence intensity.[27,28,32,33] Recent work from our group on

IR144 and IR806 showed an unusual chirp dependence when exciting the S_2 state. We observed increased S_2 emission when using transform limited pulses, whereas chirped pulses, regardless of sign, led to increased S_2 emission.[34] Here we combine chirp control and the dependence of the rate of IC on solvent viscosity,[35,36, 37] to explore, in greater detail, the role of intramolecular structural changes required in cyanine dyes to enable IC. The goal of our experiments is to achieve the largest effect on the steady-state S_2/S_1 ratio to enable novel photochemistry, solar energy capture and perhaps photodynamic therapy applications.

The organization of the paper is as follows: First, we describe the experimental details including steady state spectroscopy, lifetime measurements, and chirp dependent measurements. Second, we present steady state spectroscopy of the two cyanine dyes in different solvents along with lifetime measurements. Third, we show chirp dependent measurements for different solvents obtained at different laser intensities. Fourth, we present electronic structure calculations performed on both molecules that identify the different excited states involved as well as their equilibrium configurations. Fifth, we present a kinetic model for the observed chirp dependence. Finally, we discuss how our experimental findings, quantum calculations, and a kinetic model come together to validate our conclusions.

Results and Discussion

Results

Steady state absorption and fluorescence spectra of IR144 and IR140 in methanol, ethanol, n-propanol, ethylene glycol and glycerol are shown in Fig. 3.2a and b, respectively. The transition dipole moment representation has been adopted for both absorption and fluorescence.[38,39] The

absorption dipole strength was calculated by dividing the absorption value by its respective wavenumber $A(\nu)/\nu$. Fluorescence spectra were converted to wavenumber, multiplied by the wavelength squared and divided by the respective wavenumber cubed to calculate the fluorescence dipole strength $F(\nu) = F(\lambda)/\nu^3 \times \lambda^2$. The lower energy S_0 to S_1 transition absorption band is centered around 13,500 cm^{-1} and 12,800 cm^{-1} for IR144 and IR140, respectively. The higher energy S_0 to S_2 absorption bands are associated with two configurations that we will refer to as S_2^L and S_2^H according to their lower or higher energy transitions, respectively. The S_0 to S_2 absorption bands are ~18,400 and 19,300 cm^{-1} for IR144, and ~15,750 and 18,900 cm^{-1} for IR140. Following excitation to the S_2 excited electronic state configuration at 522 nm, the emission spectra for IR144 and IR140 show three emission bands. The fluorescence bands associated with S_2^L and S_2^H for IR144 are at 15,900 cm^{-1} and 17,000 cm^{-1}, respectively, while those for IR140 are centered at 15,500 cm^{-1} and 17,300 cm^{-1}. The S_1 emission is centered at 11,750 cm^{-1} for IR144 and 11,500 cm^{-1} for IR140.

Further analysis of the spectra in Figure 2a shows a solvatochromic shift for both the absorption and fluorescence of the S_1 excited state that is nonlinearly related to viscosity. Propanol gives the largest shift, with respect to methanol, even though glycerol has the highest polarity. Both solvent viscosity and polarity play a role in IR144 absorbance and emission band positions. Similarly, in Figure 2b IR140 shows a solvatochromic shift in both absorption and fluorescence spectra as a function of viscosity. The S_0 to S_2 absorbance increases with solvent viscosity. For both molecules, as solvent viscosity increases, the overall S_2/S_1 fluorescence ratio increases. Following excitation of S_2, emission from S_2^H is favored by IR144, whereas emission from S_2^L is favored by IR140.

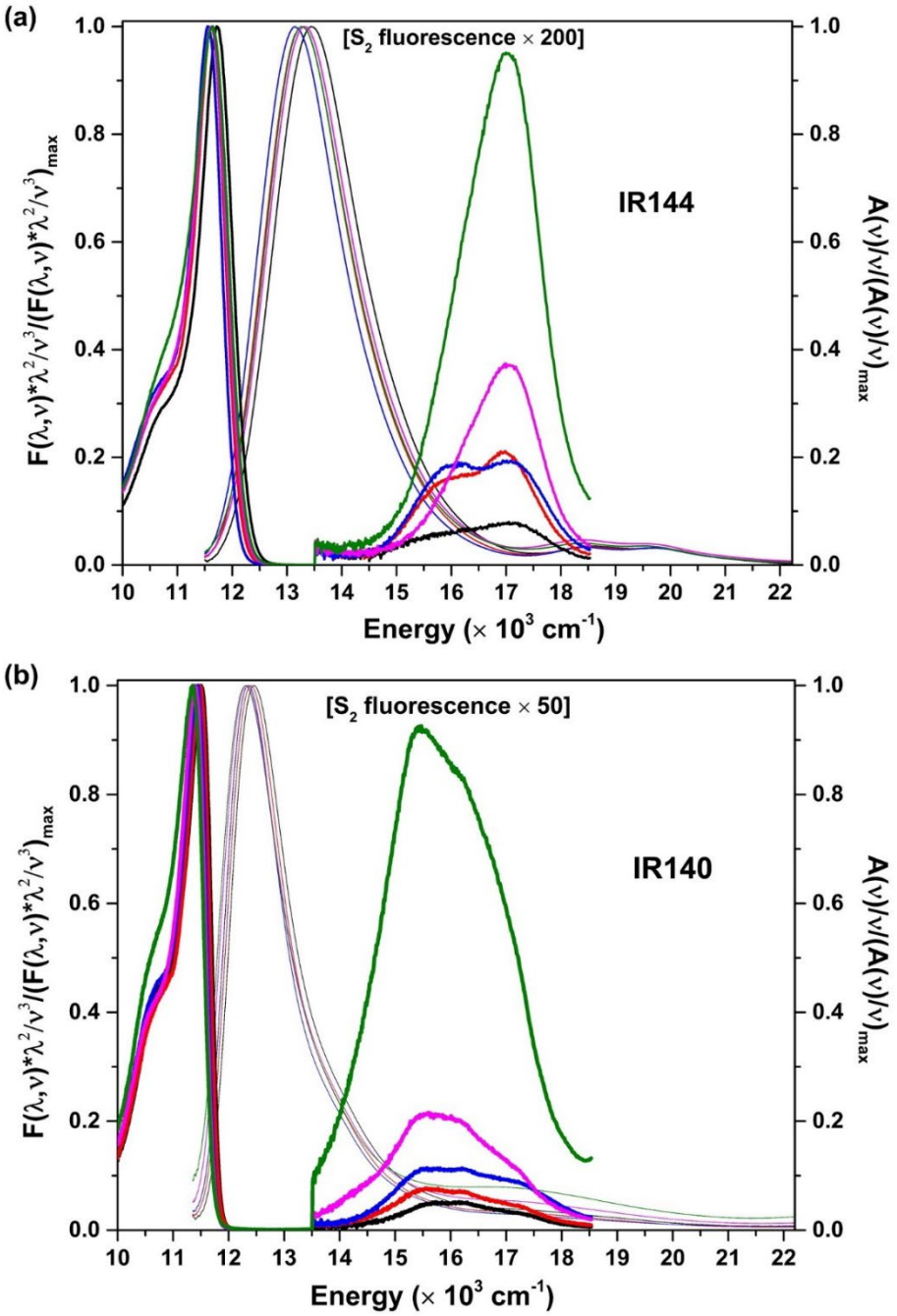

Figure 3.2: Steady-state absorption and fluorescence spectra for (a) IR144 and (b) IR140. The normalized absorption of both IR144 and IR140 is represented with thin lines whereas the normalized emission with thicker lines. Methanol, ethanol, n-propanol, ethylene glycol and glycerol are represented by black, red, blue, pink and green lines, respectively.

Excitation Emission Matrix (EEM) spectra, which record the steady-state fluorescence emission intensity as a function of excitation wavelength in a 2D contour map, were collected for both IR144 and IR140, Fig. 3.3a and b. The 400-710 nm region has been enhanced by a multiplication factor of 180 for IR144 and 150 for IR140.

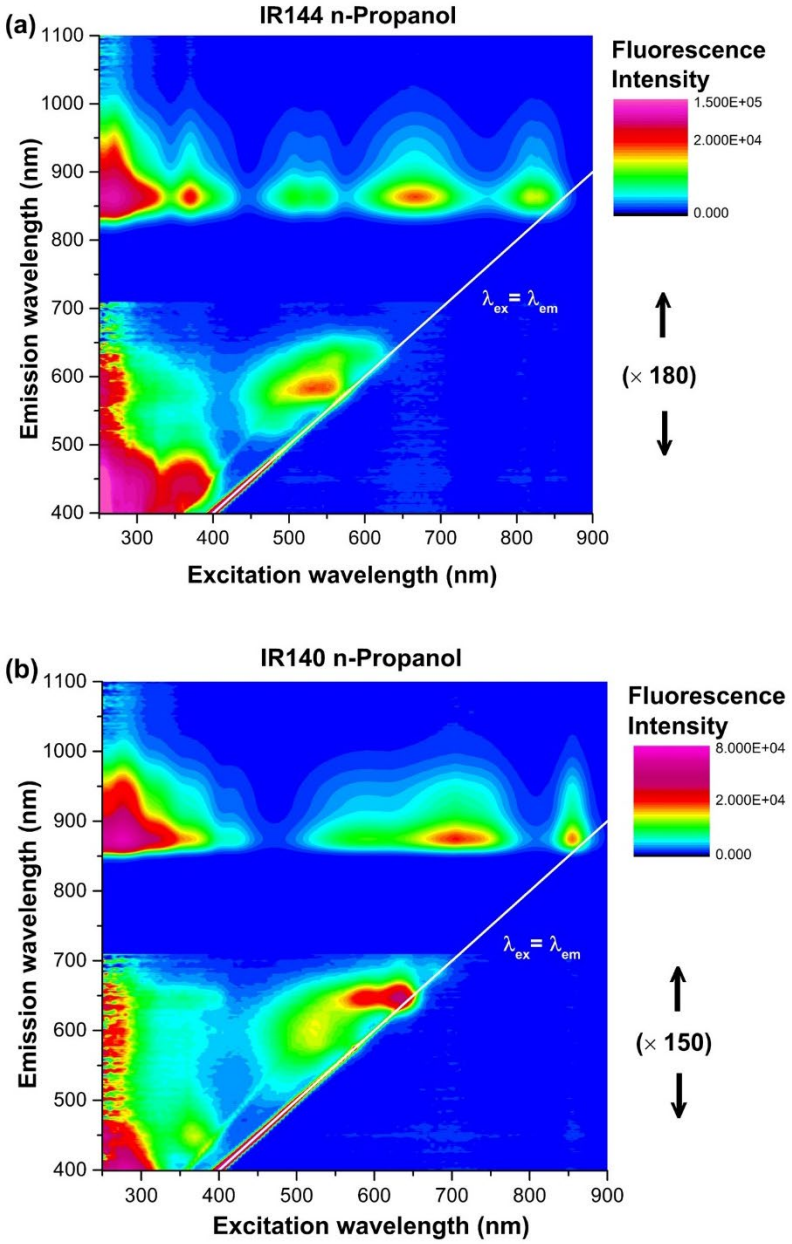

Figure 3.3: Excitation emission matrix spectra of (a) IR144 and (b) IR140 in propanol. The emission spectrum from 400 nm to 710 nm is multiplied by (a) 180 and (b) 150 for IR144 and IR140, respectively, for ease of viewing.

The EEM spectra make clear when the S_1 and S_2 excited states are reached. We also note that excitation in the 600-700 nm region for IR144 and the 650-750nm region of IR140, leads to bright emission from S_1, likely indicating the presence of an excited state that quickly relaxes to S_1.

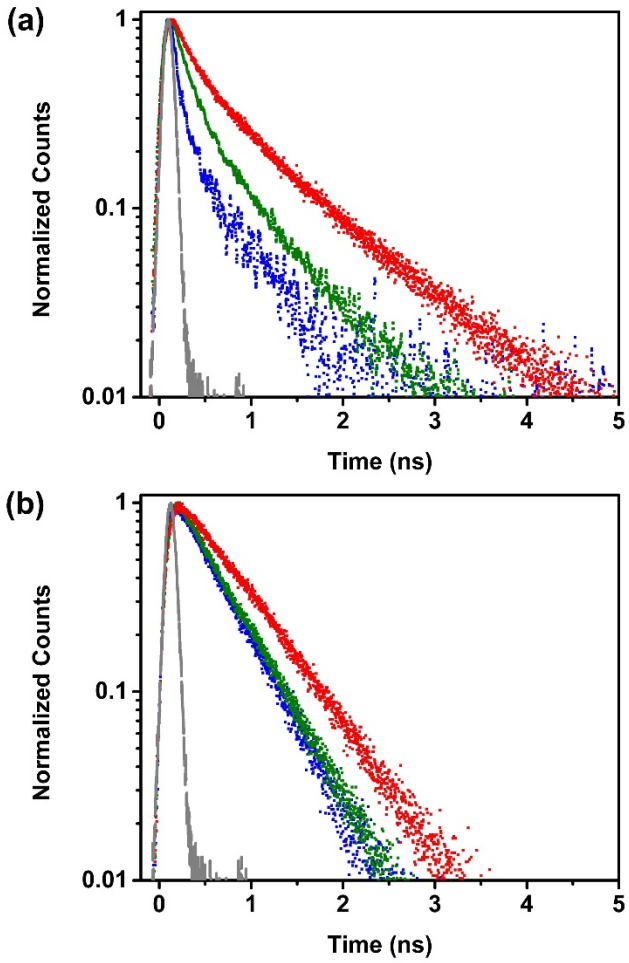

Figure 3.4: The fluorescence decay of IR144 detected at (a) S2 → S0 fluorescence maxima and (b) S1 → S0 fluorescence maxima in methanol (blue dots), ethylene glycol (green dots), and glycerol (red dots). The fluorescence lifetimes for (a) have been obtained from the function $f(t) = a_1 \exp(-t/\tau_1) + a_2 \exp(-t/\tau_2)$ while for (b) have been obtained from the function $f(t) = b_1 \exp(-t/\tau_3) - b_2 \exp(-t/\tau_4)$. The time constants have been obtained post deconvolution of the IRF from the fluorescence decay signals.

Fluorescence lifetime measurements, with an excitation wavelength of 531 nm were carried out in IR144 and IR140 solutions in methanol, ethylene glycol and glycerol. Fig. 3.4a and 3.4b show fluorescence lifetime measurements from IR144 S_2 and S_1 states, respectively. The S_2 emission is characterized by a biexponential decay, that is likely associated with the competition between fluorescence from S_2 and IC to S_1. The S_2 emission lifetime is observed to increase with solvent viscosity. The S_1 emission signal shows a rise followed by a decay, with both lifetimes

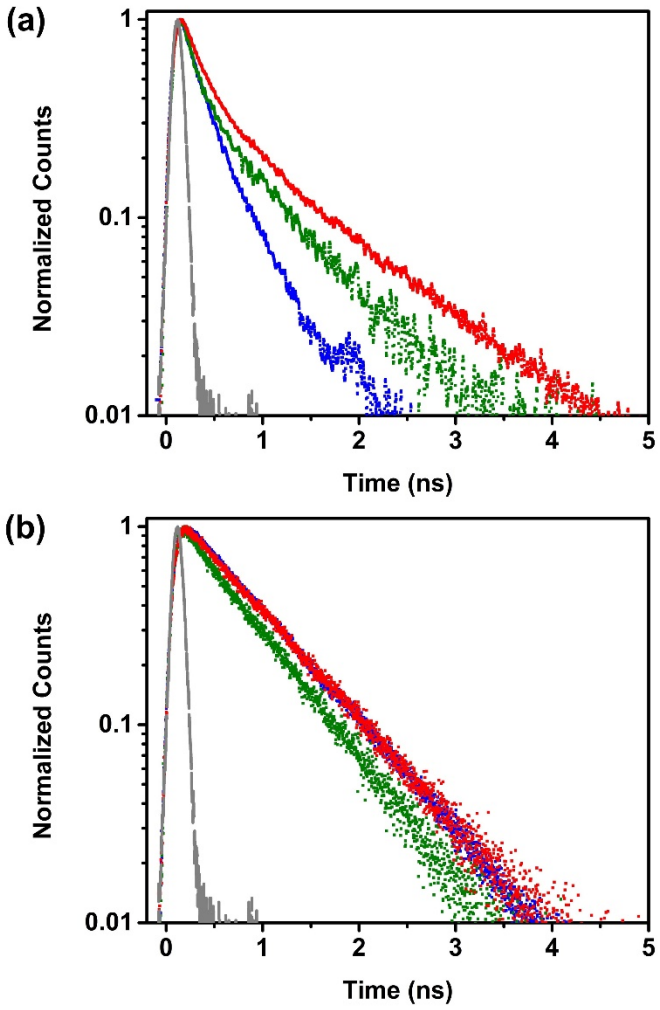

Figure 3.5: The fluorescence decay of IR140 detected at (a) S2 → S0 fluorescence maxima and (b) S1 → S0 fluorescence maxima in methanol (blue dots), ethylene glycol (green dots), and glycerol (red dots). The fluorescence lifetimes for (a) have been from the function $f(t) = a_1 \exp(-t/\tau_1) + a_2 \exp(-t/\tau_2)$ while for (b) have been obtained from the function $f(t) = b_1 \exp(-t/\tau_3) - b_2 \exp(-t/\tau_4)$. The time constants have been obtained post deconvolution of the IRF from the fluorescence decay signals.

increasing with solvent viscosity. Fig. 3.5a and 3.5b show fluorescence lifetime measurements from IR140 S_2 and S_1 states, respectively, for IR140. The S_2 fluorescence lifetime increases with viscosity for IR140 and IR144. Interestingly, the IR140 S_1 fluorescence lifetime does not follow the same viscosity trend. We find the fluorescence lifetime for IR140 in methanol to be similar to that in glycerol.

Table 1: Fluorescence lifetimes obtained from time-correlated single photon counting experiments. The time constants are as defined in Fig. 3.4 and 3.5.

Molecule	Solvent[a]	a_1	τ_1 (ps)	a_2	τ_2 (ps)	τ_3 (ps)	τ_4 (ps)
IR144	MeOH	0.86	46 ± 1	0.14	452 ± 10	455 ± 2	32 ± 3
	EG	0.78	175 ± 2	0.22	682 ± 14	456 ± 1	43 ± 3
	Gl	0.60	221 ± 4	0.40	932 ± 13	630 ± 2	48 ± 3
IR140	MeOH	0.52	107 ± 3	0.48	347 ± 5	730 ± 2	44 ± 1
	EG	0.71	124 ± 2	0.29	687 ± 9	617 ± 2	26 ± 1
	Gl	0.69	174 ± 2	0.31	914 ± 11	726 ± 2	42 ± 1

[a] Abbreviations: MeOH = Methanol, EG = Ethylene Glycol, Gl = Glycerol.

Femtosecond chirp scans, from negative values (higher before lower frequencies) to positive values (lower before higher frequencies) were carried out on IR144 and IR140 in methanol, ethanol, and propanol. The excitation pulse, with near Gaussian spectrum and a central wavelength near the S_2 absorption band, for both IR144 and IR140 is chirped while fluorescence spectra spanning both excited states are collected. Fig. 3.6a and b show the trend in S_1 and S_2 integrated fluorescence with increasing chirp for IR144 and IR140, respectively. The y-axis is the relative change in integrated fluorescence, with respect to TL fluorescence.

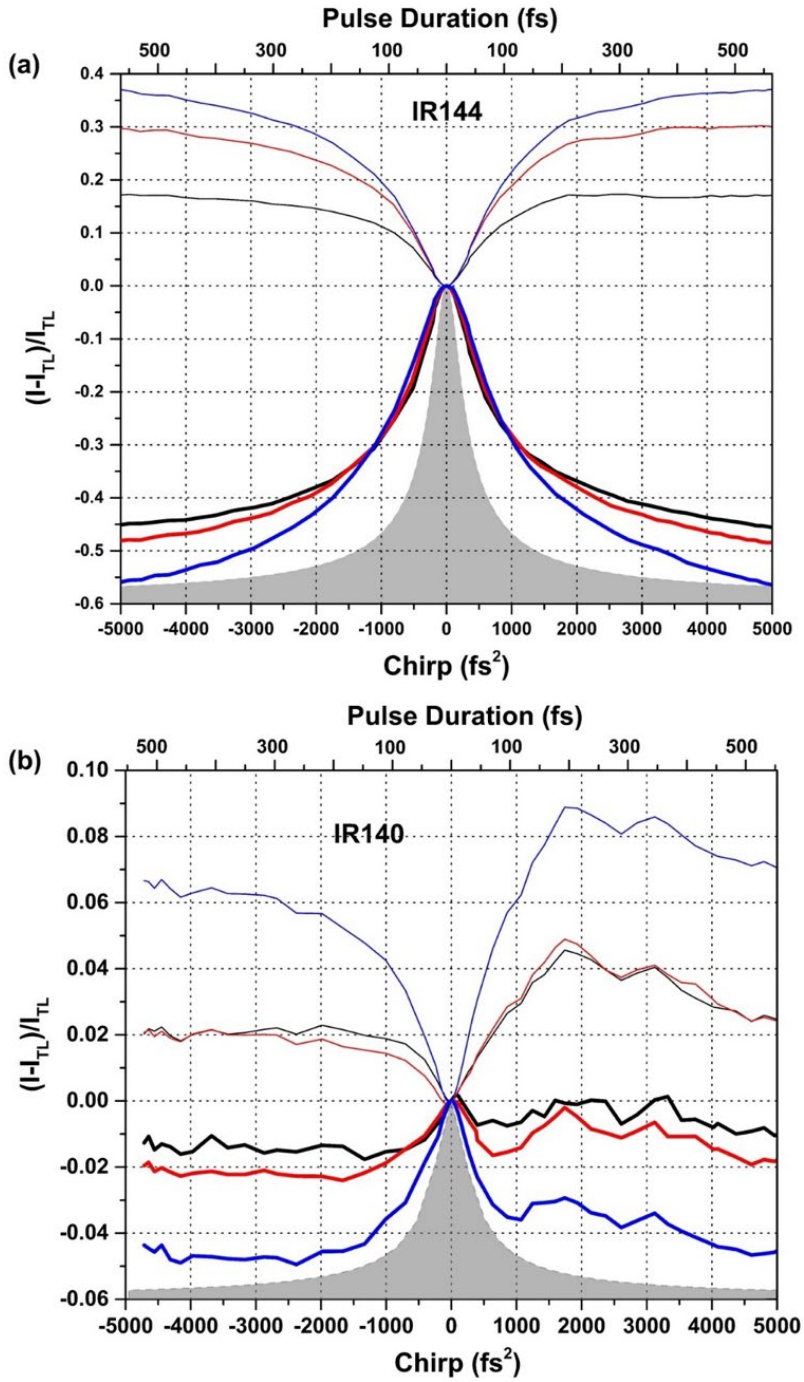

Figure 3.6: Chirp dependence scans conducted on (a) IR144 and (b) IR140 from -5000 fs^2 to +5000 fs^2 at constant laser power for each molecule. (For IR140, a lower laser power intensity was used) The fluorescence intensity for each chirped pulse was measured against the transform limited fluorescence for each respective energy state (S_2 and S_1) to display. Methanol, ethanol and n-propanol are represented by black, red and blue lines, respectively. S_1 and S_2 are represented by thin and thick lines, respectively.

As shown in Fig. 3.6, the resulting increase in S_2 and decrease in S_1 fluorescence at near zero chirp are nearly symmetrical with respect to chirp magnitude, which is similar to previous experiments from our group. This chirp dependence is unusual. As mentioned in the introduction, excitation with negatively chirped pulses should lead to a pronounced decrease in fluorescence compared to excitation with positive chirped pulses. It is important to note here, that the total integrated S_1 fluorescence is considerably higher than the total integrated S_2 fluorescence (see Fig. 3.2). Therefore, S_1 fluorescence changes at TL represent a considerable decrease in fluorescence yield, whereas the S_2 fluorescence increase at TL involves much smaller fluorescence values. The shaded gray outline, located on the bottom half of Fig's 3.6a and 3.6b, represents the SHG dependence as a function of chirp obtained with the experimental pulses. The dependence of SHG on chirp is proportional to the inverse of the pulse duration of the chirped pulses, $\tau_{out,}$ given by Equation (1). In this equation, τ_{in} is the input pulse, $f = 4*\ln 2$, and φ_2 is the amount of chirp

$$\tau_{out} = \tau_{in}\sqrt{1 + f^2\left(\frac{\varphi_2}{\tau_{in}^2}\right)^2} \qquad (1)$$

Because the observed response to chirped pulses following S_2 excitation in cyanines is unusual, we extend our previous work to solvents with higher viscosity values using methanol, ethanol, and propanol solutions. We find that as the viscosity increases, the effect that chirped pulses elicit on fluorescence increases in magnitude for both S_1 and S_2. In IR144, the same chirp dependent symmetrical S_2/S_1 enhancement for TL pulses is apparent for each solvent. For IR140, the S_2/S_1 ratio increase is observed near zero chirp, but the dynamics observed are less symmetric with respect to chirp. We note a slight increase in S_1 and S_2 emission for positively chirped pulses, as compared to negatively chirped pulses. The lower fluorescence for negatively chirped pulses is reminiscent of the chirp dependence observed in first excited states showing

depleted fluorescence for negatively chirped pulses due to stimulated emission.[27,28,29,30,31,32] One can understand the asymmetry by considering a negatively chirped pulse experiment as one where a shorter wavelength pulse launches the wave packet in the S_2 excited and a longer wavelength pulse bringing the wavepacket back to the ground state.

One can get a sense of the wavepacket motion dynamics in the S_2 state using Eq. (1) to calculate the corresponding pulse duration on the top x-axis (Figure 6 and 7). Given that the chirp dependence of the S_2 fluorescence emission has a Lorentzian dependence on chirp, like the SHG dependence. Taking the inverse of Eq. (1) with adding fitting parameters *h*, and *b*, corresponding to the amplitude and baseline results in Eq. (2), which can be used to fit the S_2 chirp curves obtained for the different solvents (in Fig. 3.6) and obtain a fitting parameter τ_c that can be used to calculate changes in wavepacket dynamics. When $\tau_c = \tau_{in}$, we recover the experimental SHG intensity dependence. When the radical in the denominator equals 2, it implies that the chirped pulse has doubled in duration, and from then on, pulse duration increases linearly with chirp. We have chosen this point, when a chirped pulse can be considered analogous to two separate pulses with different central frequency, to define the 'wavepacket motion' time, a parameter that is proportional to the wavepacket motion dynamics in the different solvents. The resulting parameters are in Table 2, along with a 'wavepacket motion' obtained by solving Eq. 2 for each of the τ_c values. The numbers in Table 2 allow us to get a sense of the delayed wavepacket dynamics in the different solvents resulting from the increased viscosity.

$$y = b + \frac{h}{\sqrt{1 + f^2\left(\frac{\varphi_2}{\tau_c^2}\right)^2}} \qquad (2)$$

Table 2: Fitted chirped S_2 fluorescence curves were fitted with a Lorentzian line-shape.

Molecule	Solvent	Width (fs)	Error
IR144	Methanol	35.3	± 0.4
	Ethanol	38.3	± 0.36
	n-Propanol	43.4	± 0.34

Power-dependence experiments were conducted in methanol solutions for both dyes, as shown in Fig. 3.7. With the increase in laser power the S_2 intensity appears to saturate for both dyes at a laser power of 15mW. At the highest intensity, maximum S_2 emission is no longer observed for TL pulses. Notice that saturation is not observed for S1 fluorescence. We find the observed chirp dependence of the S_2 state in IR144 is significantly greater than the effect observed in IR140.

Having shown that viscosity causes a higher S_2/S_1 emission ratio in both IR144 and IR140, especially for TL pulses, we explore a possible relationship with chirp and laser intensity on the S_2 emission spectra of the molecules (Figures 8a and 8b). Measurements were repeated for three laser powers, 10, 15, and 20 mW. The pulses were TL (black), positively (red), or negatively (blue) chirped. For IR144, when excited by TL pulses, we find that the three intensities produce the same spectrum which corresponds to S_2^H . For chirped pulses, we find that the blue shifted S_2^H emission is less intense but increases with laser pulse intensity. This trend is not observed in IR140 (Figure 8b); in fact, results for 10 and 15 mW for TL and chirped pulses produced identical spectra. This is consistent with IR140 preferring emission from the S_2^L configuration.

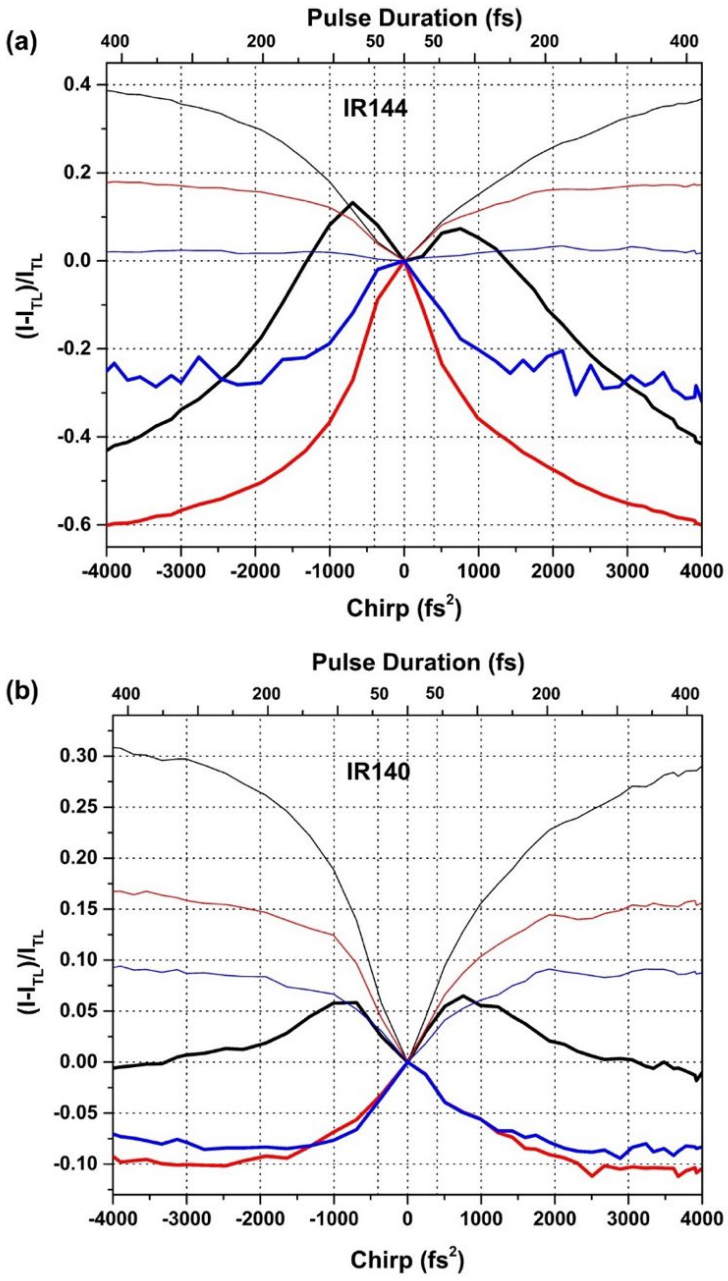

Figure 3.7: Chirp dependence scans carried out as a function of laser intensity for (a) IR144 and (b) IR140 in methanol. Relative fluorescence change (from TL) of S_1 and S_2, with respect to chirp is plotted for differing laser power values. Laser excitation power of 15mW, 10mW and 5mW are represented by black, red and blue lines, respectively. S_1 and S_2 variations are represented by thin and thick lines, respectively.

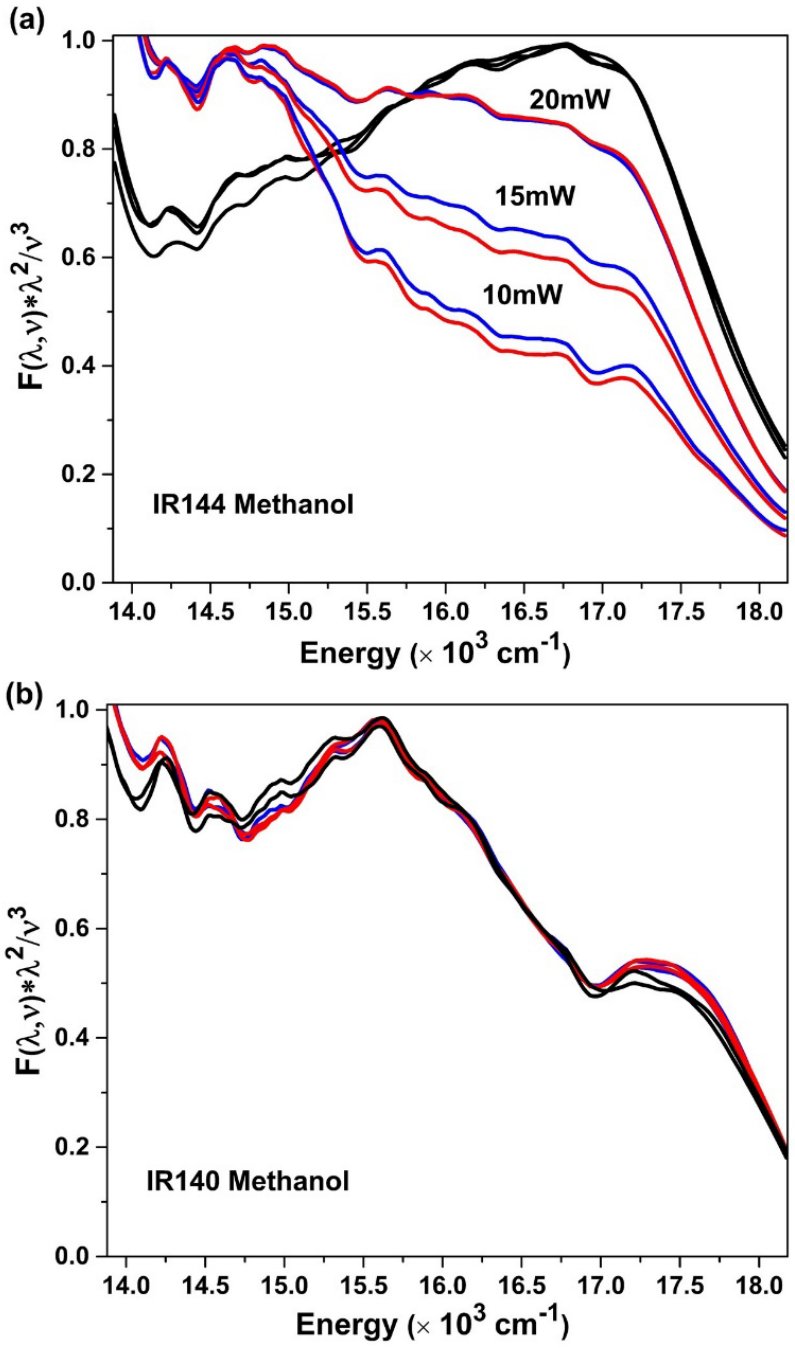

Figure 3.8: Normalized S_2 fluorescence spectra are plotted as a function of chirp and power value for (a) IR144 and (b) IR140. The blue line (positive chirp) considers chirp values from +4000 fs^2 to +5000 fs^2, while the red line (negative chirp) averages the fluorescence spectrum from -4000 fs^2 to -5000 fs^2. The black line (transform-limited pulses) stays relatively the same as the power increases for both dyes. The (b) IR140 fluorescence spectrum is not dependent upon chirp or power. 15mW and 10mW S_2 spectra are shown for the three differing pulse descriptions, with relatively no change. The data have been normalized to the highest value within the S_2 fluorescence emission band.

The motivation of this work is to maximize the lifetime of S_2 by preventing or delaying IC to S_1 so that the excess energy is available for photochemical processes such as solar capture or therapeutic applications. Therefore, we quantify the integrated S_2/S_1 fluorescence ratio observed for IR144 and IR140 in the different solvents by steady state fluorescence spectroscopy as well as by femtosecond TL and chirped pulses in Table 3. Increasing solvent viscosity increased the S_2/S_1 ratio by a factor of 8.6 and 21 for IR144 and IR140, respectively. Femtosecond TL pulses caused even higher enhancement in the S_2/S_1 ratio by a factor of 39 and 47 for IR144 and IR140, respectively. When taking obtaining the change in the S_2/S_1 ratio obtained for femtosecond chirped pulses for methanol and TL pulses for glycerol, we obtain an overall effect of 86 and 55 for IR144 and IR140, respectively. The large difference in the effect observed for femtosecond pulse excitation compared to steady state spectroscopy indicates an additional pathway for the excitation that populates S_2 as will be discussed below.

Table 3: S_2/S_1 integrated fluorescence intensity ratios.

Molecule	Solvent	Viscosity (cP)	Steady state	TL pulses	Chirped pulses
IR144	Methanol	0.05435	0.0014	0.022	0.010
	Ethanol	1.095	0.0035	0.0342	0.013
	n-Propanol	2.256	0.0040	0.045	0.015
	Ethylene glycol	16.2	0.0047	0.030	0.025
	Glycerol	648	0.012	0.86	0.82
IR140	Methanol	0.05435	0.0051	0.027	0.023
	Ethanol	1.095	0.0081	0.023	0.021
	n-Propanol	2.256	0.014	0.028	0.025
	Ethylene glycol	16.2	0.025	0.10	0.10
	Glycerol	648	0.11	1.27	1.19

Theory

Time-dependent density functional theory (TD-DFT) calculations were performed to identify the absorption and emission transitions of IR140 and IR144 molecules. Though TD-DFT calculations are known to predict excitations energies with errors of several tenths of an eV in cyanine dyes, the shapes of potential energy surfaces are typically found to be very accurate.[40,41] All calculations were performed with the TeraChem software package.[42,43,44] Geometries were optimized at the CAM-B3LYP[45]/6-31G* level. Except where noted otherwise, all calculations were performed using an implicit model of the glycerol solvent (conductor-like polarizable continuum model, C-PCM,[46,47] with dielectric constant $\varepsilon = 46.5$). All calculations were repeated in implicit methanol ($\varepsilon = 33.0$), with effectively identical results, except as noted specifically below. Alkyl chains over three carbons long and any associated sulfonate groups were replaced by methyl groups to save computational expense. Ground state optimizations show that the s-trans conformers have a lower ground state energy than the s-cis conformers for both molecules. In both molecules, the central amine group was found to rotate out of the plane of the polymethine chain. Excited state optimizations were performed to identify possible emissive geometries. The results of these optimization are presented in Figures 3.9 and 3.10 for IR140 and IR144, respectively. Three low-lying states were examined in both IR140 and IR144, which we will label S_1, $S_{1.5}$, and S_2. Optimized structures in methanol, glycerol, and vacuum can be found in the supporting information.

The computed S_1 vertical excitation energies at the Franck-Condon point (S_0min) are 2.37 eV and 2.54 eV for IR140 and IR144, respectively. These overestimate the respective experimental absorption maxima (1.54 eV and 1.67 eV in methanol) by 0.83 and 0.87 eV, respectively. Thus, we apply respective shifts of the excited state potential energy surfaces of -

0.83 and -0.87 eV in our analysis of the computational data below. These shifts account both for well-known errors in TD-DFT excitation energies and for the different environment in our calculations compared to experiment (i.e., the absence of charged sulfonate groups, counterions, and hydrogen bonding interactions with solvent).

The S_1 minimum was identified in each dye, which we label S_1min. In both cases, S_1min is very similar to S_0min, and has a vertical S_0-S_1 gap less than 0.1 eV smaller than that at S_0min. The shifted theoretical S_1 emission energies are in excellent agreement with experiment: 1.44 eV (2.27 eV unshifted) and 1.51 eV (2.38 eV unshifted) for IR140 and IR144, respectively, compared to experimental values of 1.44 eV and 1.48 eV. Optimization on $S_{1.5}$ did not yield a distinct minimum. Instead, it is found that S_1 and $S_{1.5}$ intersect, which likely facilitates efficient nonradiative decay from $S_{1.5}$ to S_1. Thus, no emission is expected from $S_{1.5}$.

In both IR140 and IR144, two distinct local minima were found on S_2, which we label S_2min-1 and S_2min-2. As detailed below, in both systems the computed S_0-S_2 energy gaps at these minima are in good agreement with the experimentally observed S_2^H and S_2^L emission peaks. In addition, in both IR140 and IR144, both S_2min-1 and S_2min-2 are significantly distorted compared to the S_0min structure. Of the two minima, S_2min-1 is more analogous to the Franck-Condon geometry; the polymethine chain remains planar, but the central amine group is twisted to 77° and 73° in IR140 and IR144, respectively (compared to 37° and 43° at S_0min). In the more distorted S_2min-2, the polymethine chain itself is twisted by 91° and 94°, relative to the planar S_0min structure. For comparison, the S_1min is less distorted, with a planar polymethine chain and respective twist angles about the central amine group of 50° and 59°.

These significant distortions of the emissive geometries compared to the S_1min structures explain the observed solvent viscosity dependence of the ratio of S_2 to S_1 emission in both IR140

and IR144. Upon excitation to the S_2 state, molecules will be trapped at the distorted S_2 minima by more viscous solvents and emit from S_2 before nonradiative decay can occur. Thus, the ratio between S_2 and S_1 emission intensity grows larger with increasing solvent viscosity.

Careful analysis of the S_2 PES sheds light on the origin of the distinct $S_{2min\text{-}1}$ and $S_{2min\text{-}2}$ emission peaks. We believe that these two minima correspond to the experimentally observed S_2^H and S_2^L emission. In IR144, the predicted emission energies are 2.18 and 1.89 eV (3.05 and 2.76 eV unshifted) at $S_{2min\text{-}1}$ and $S_{2min\text{-}2}$, respectively. These values are in good agreement with the experimentally observed emission peaks at 2.11 and 1.98 eV, respectively. Optimization in implicit methanol solvent provides nearly identical minima and emission energies. Thus, we suggest that S_2^H and S_2^L emission correspond to the excited state structures that are twisted about either the amine substituent or the polymethine chain, respectively.

For IR140 in glycerol, two distinct minima (S_2min-1 and S_2min-2) are observed as well. The computed emission energies are 2.63 and 2.08 eV (3.46 and 2.91 eV unshifted). These likely correspond to the experimentally observed S_2^H and S_2^L emission peaks at 2.01 and 1.92 eV, though agreement with the computationally predicted feature at 2.63 eV is only qualitative. In addition, only a single minimum (similar to S_2min-2) was observed upon optimization in implicit methanol solvent. Given the large number of degrees of freedom on the molecule, there may be an addition minimum on S_2 that we have not found in our study. However, given the similarity of both the experimental emission spectra and the computed PESs of IR140 and IR144, it appears likely that the S_2^H and S_2^L emission peaks arise from distinct minima on S_2 in both systems.

Comparison of the S_2-$S_{1.5}$ energy gaps at the optimized S_2 minima provides insights into the relative ratios of S_2 to S_1 emission in these systems. In IR144, relatively small gaps of 0.54 and 0.21 eV are predicted at the S_2min-1 and S_2min-2, respectively. This suggests relatively fast

non-radiative relaxation to $S_{1.5}$, and subsequently to S_1 (through the above-mentioned intersection), which is consistent with the relatively low ratio of S_2 emission to S_1 emission in this system. The gaps are larger in IR140 (1.25 and 0.69 eV), consistent with the higher yield of S_2 emission relative to S_1. The underlying raw calculations supporting the theory are provided in the Supporting Information Tables S1-S6.

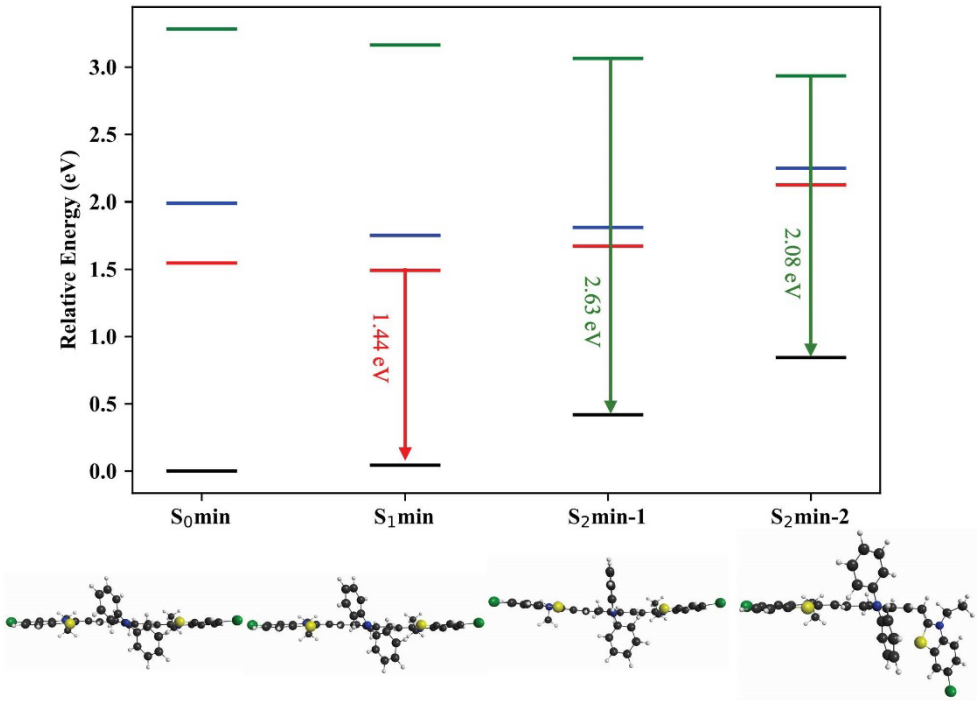

Figure 3.9: Computed state energies of IR140 in glycerol at corresponding geometries. S_0, S_1, $S_{1.5}$, and S_2 energies are shown by black, red, blue and green lines, respectively. Energies for S_1, $S_{1.5}$, and S_2 are shifted as described in the text.

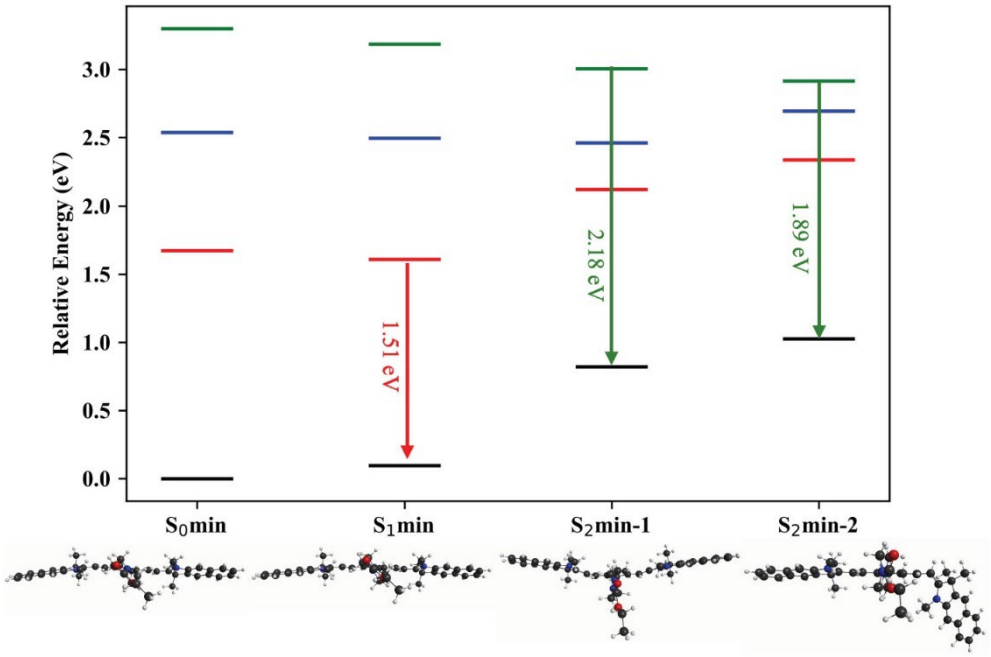

Figure 3.10: Computed state energies of IR144 in glycerol at corresponding geometries. S_0, S_1, $S_{1.5}$, and S_2 energies are shown by black, red, blue and green lines, respectively. Energies for S_1, $S_{1.5}$, and S_2 are shifted as described in the text.

Numerical Simulations

Numerical simulations were carried out in order to understand the chirp dependence observed experimentally, and how that dependence varies with the solvent viscosity and laser intensity. The simulations are based on the scheme shown in Figure 3.11. The first step being excitation from S_0 to the FC region of S_2, forming the wavepacket shown in red. From there, the wave packet relaxes to either of the S_2 state configurations with rate k_{r2} or crosses over to S_1, by way of a conical intersection between the two states, with an IC rate k_{IC} and relaxes to the bottom of S_1 with rate k_{r1}. Once the fluorescence lifetimes for S_1 and S_2 of 452 ps and 455 fs, respectively, for IR144 are added to the simulation, the set of four linear differential equations is solved using Mathematica® and the results closely resemble the experimental lifetime decay

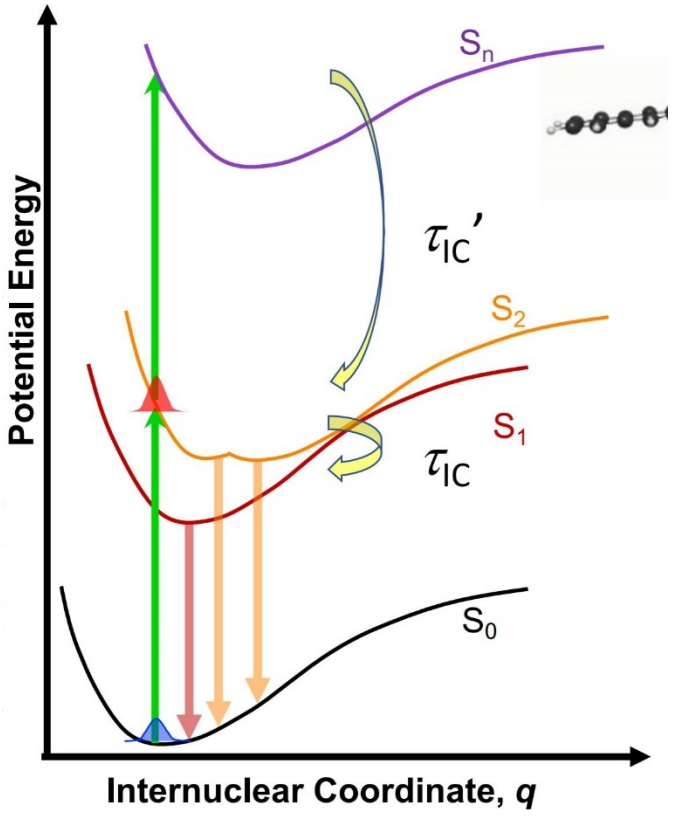

Figure 3.11: Schematic model representing potential energy curves that illustrate the different processes involved in the femtosecond chirped pulse experiments.

measurements for methanol. For these calculations, the population starts in S_2 and the rates $1/k_{r1}$, $1/k_{r2}$, $1/k_{IC}$ are 2 ps, 2 ps, and 0.5 ps, respectively. In order to keep the model as compact as possible, we did not introduce state $S_{1.5}$, and no efforts were made to differentiate the model to differentiate between IR144 and IR140.

To simulate the chirp dependence results, we include the possibility of two-photon excitation from the FC region reached by the first photon to a higher excited state (see Fig. 3.11), which empirically relaxes preferentially to S_2 via IC. When the pulses are TL, the probability of two-photon excitation is maximum, and as the chirp magnitude increases, the two-photon excitation pathway is suppressed. Because two-photon excitation is proportional to pulse duration, we set $1/k_{r2}$ proportional to the chirp-dependent pulse duration. By including this dependence, k_{r2} controls how much population goes into S_2,

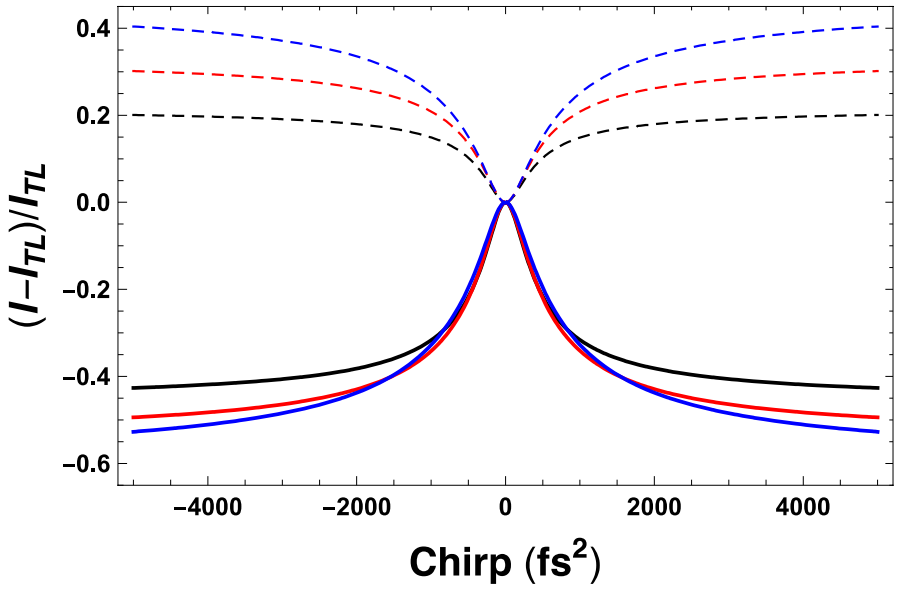

Figure 3.12: Results from numerical simulations of the S_1 and S_2 populations as a function of chirp and viscosity. The viscosity of the solvent affects the rate of IC and this is reflected in the chirp dependence. Results shown for methanol (black), ethanol (red), and propanol (blue), where the only parameter changed in these simulations was the viscosity of the solvent.

either by direct relaxation from the FC region or via two-photon excitation. With this addition, the S_1 and S_2 populations mimic the behavior, as observed in the experiments, without the need to introduce higher excited states or additional relaxation constants. Given that wavepacket dynamics and changes in the molecular geometry required for IC proceed at a rate proportional to the viscosity of the solvent, we made $1/k_{IC}$ directly dependent on viscosity. This explains why the observed chirp dependence becomes broader as viscosity increases. Our experiments were found to be very sensitive to laser intensity. When the laser power is very low, the effect of chirp on the pulses is smaller and nonlinear processes are no longer possible. Here, chirp makes no difference. Because S_2 is nested within S_1, as illustrated in Fig. 3.11, laser excitation populates both the S_1 and S_2 states. In our numerical calculations, the initial population of S_1 was set to 5 times greater than that of S_2. With these parameters, we were able to reproduce the chirp and viscosity dependence observed experimentally for methanol, ethanol and propanol, as shown in Figure 3.12. For the simulations shown, the only parameter that was changed was the viscosity of the solvent.

Saturation of the S_2 FC region occurs under high laser intensity, near TL conditions. In this case, as the pulse duration increases, the wavepacket has time to move out of the FC region and S_2 can achieve greater population than observed with TL pulses. As pulse duration increases further, the behavior returns to the unsaturated case. Saturation was simulated by multiplying the population of S_2 by a k_{r2}-dependent Gaussian function representing the laser pulse with an additional contribution controlled by the rate of depopulation from S_2 to S_1. This additional population is rationalized because two-photon excitation may occur for the population that has undergone IC to S_1, when the laser intensity is very high. The simulations as a function of laser intensity, using the viscosity of methanol, are presented in figure 3.13. We did not include in our

model the wavepacket motion in the S_2 state that results in the asymmetry visible in the IR140 data, namely, greater fluorescence intensity for positively chirped pulses compared to negatively chirped pulses.

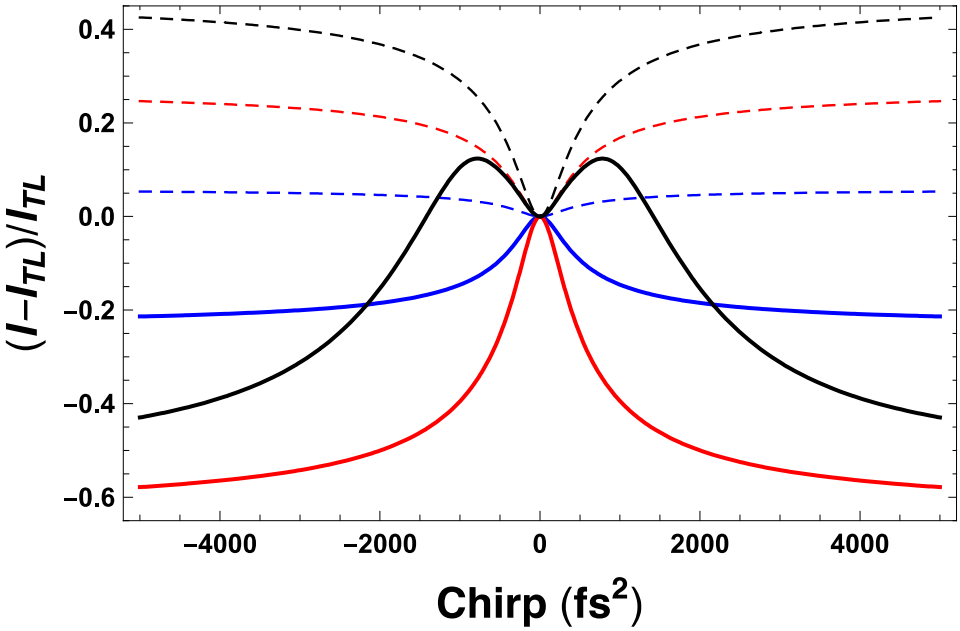

Figure 3.13: Results from numerical simulations of the S_1 and S_2 populations as a function of chirp for three different laser intensities: weak pulses (blue), higher intensity (red), and saturation (black); as described in the text.

Discussion

Results from steady state spectroscopy, including EEM spectra and fluorescence lifetime measurements in IR144 and IR140 in different solvents can be understood by taking advantage of the quantum calculations presented here. While emission from S_1 and S_2 states had been observed before, here we report on two distinct molecular configurations for the S_2 state, and the preference of IR144 to emit from S_2^H and that of IR140 from S_2^L. These peaks correspond to differently twisted minima on the S_2 surface. The EEM spectra reveal absorption by an intermediate electronic state between S_1 and S_2 that emits exclusively from S_1. Quantum

calculations are able to predict this state and in addition find that it relaxes to the S_1 equilibrium geometry, consistent with the experimental data. Fluorescence lifetime measurements demonstrate the relatively long-lived S_2 states of these molecules, their dependence on viscosity, and rate of IC down to the S_1 state. These measurements are later used to parametrize numerical simulations.

Chirp dependence measurements for solvents with different viscosity revealed that the S_2/S_1 ratio is maximized for TL pulses, as had been observed before by our group. However, we find that the dependence on chirp shows that the IC dynamics are slowed by more viscous solvents. The slowdown can be understood by realizing that significant molecular geometry changes are required for the process. We find that the slowdown is even more pronounced for IR140 than for IR144, and this can be explained by the favored polymethine twist as compared to amine substituent twist, respectively.

Most importantly, the enhanced S_2/S_1 ratio for TL pluses can now be understood as a two-photon excitation originating from the FC region reached by the first photon, provided the wavepacket has not moved during the excitation process. This conclusion is reached by correlating multiple observations. First, the EEM spectra in Fig. 3.3, show that indeed there is an electronic state reachable by two-photon 520 nm excitation (260 nm one-photon), and that excitation of that state leads to $S_2 \rightarrow S_0$ emission. Power dependence measurements of the S_2/S_1 ratio (Fig. 3.7) are also consistent with two-photon excitation. Numerical simulations based on a kinetic model allowed us to test several alternative processes and their dependence on laser intensity, pulse chirp, and solvent viscosity. The overall scheme depicted in Fig. 3.11 is the only one that could accurately simulate solvent viscosity (Fig. 3.12), and laser intensity (Fig. 3.13).

Conclusion

In this study we have applied femtosecond pulse chirp and solvent viscosity to manipulate the rate of IC following S_2 excitation of IR144 and IR140. Steady state spectroscopy including excitation emission spectra and fluorescence lifetime emission, together with quantum calculations have revealed an excited state termed $S_{1.5}$, that promptly relaxes to S_1 but influences the IC process from S_2. In addition, we find that the S_2 state has two stable molecular configurations S_2^H and S_2^L associated with amine substituent twist or polymethine chain twist, respectively. We find that IR144 emits preferentially from S_2^H, while IR140 emits preferentially from S_2^L. Taking advantage of solvent viscosity and femtosecond pulse chirp, we are able to manipulate the S_2/S_1 fluorescence ratio of IR144 from a minimum value of 0.01 for methanol with 5000 fs^2 chirp, to a maximum of 0.86 obtained for TL pulses. This overall change corresponds to almost two-orders of magnitude. The ability to control IC from upper excited states, may open exciting possibilities for the photochemical applications of cyanine dyes in imaging and photodynamic therapy. The results presented here may lead to future work on manipulating the lifetime of the upper excited states of similar polymethine dyes, other cyanine dyes and possibly other molecules such as carotenes.

FINAL CONCLUSIONS AND FUTURE RESEARCH

Conclusions

The purpose of this research experiment was to analyze the dual effect of viscosity and pulse chirp on excited state dynamics in cyanine dyes. This led to the finding that increasing solvent viscosity increases the S_2/S_1 ratio, increasing photon density increases the S_2/S_1 ratio and increasing both produces a multiplicative effect. Increased photon density also increases the likelihood of two-photon excitation, a non-linear optical process we determined is most-likely responsible for the S_2/S_1 increase at TL. In addition, it was found that both IR144 and IR140 have two S_2 fluorescent peaks and they can be selected for in IR144.

When increased S_2/S_1 fluorescence ratios for IR144 are observed, either as viscosity or photon density is increased, there is an increase in the S_2^H fluorescence peak in comparison to the S_2^L peak. This reveals a different relaxation pathway that results in higher S_2 fluorescence values. This S_2 peak selection is not observed in IR140. As the S_2/S_1 fluorescence ratio increases, the lower energy S_2 peak is always favored and the S_2^H to S_2^L ratio stays relatively constant during these changes.

In conclusion, it was found that non-linear absorption and a decreased IC rate resulted in increased S_2/S_1 ratios in both IR144 and IR140. For IR144, chirped pulse excitation in methanol compared to TL in glycerol increased the S_2/S_1 fluorescence ratio by a factor of 86. In IR140, chirped pulse excitation in methanol versus TL in glycerol increased the S_2/S_1 ratio by 55. While steady state excitation in methanol compared to glycerol gave an 8.6 and 21.6 factor increase in the S_2/S_1 ratio for IR144 and IR140, respectively. This reveals the multiplicative effect viscosity and photon density together have on increasing the S_2 fluorescence yield in cyanine dyes.

Here, it is shown that environmental factors such as viscosity and laser-controlled photon density can be utilized to influence fluorescence yield and wavepacket pathway selection in cyanin dyes and possibly other fluorophores. This is significant because it allows for the control of the S_2/S_1 fluorescence ratio. As S_2/S_1 increases, the energy being emitted from the molecule, in the form of light, is increased since S_2 is a higher energy state than S_1. This type of control can be applied to many different processes, one example is solar energy. Within solar energy, one of the main limitations is the efficiency of the solar cells. Cyanine dyes have been implemented as solar cells because of the charge associated with their side chain causing them to have semiconductor properties. Solar cells or panels are limited by their energy band gap. Here, it is shown that with increased S_2/S_1, a considerable amount of S_2 fluorescence can be emitted from these dyes increasing the band gap from the S_1 to S_0 transition to the S_2 to S_0 transition. This increases the energy band gap by almost 50%. The hope is, although the focus here was very fundamental, further research in this area would contribute to the application of this finding within the renewable energy realm.

Further Research

Further research on other dyes utilizing both solvent viscosity and laser pulse chirp synchronously could be employed to further understand higher excited state dynamics. Other environmental factors such as pH, ionic solutions and temperature could be exploited in use with cyanine dyes to better understand their effect on the S_2/S_1 fluorescence ratio. Excitation to S_3 with analysis of how all three fluorescence ratios are influenced by viscosity and photon density would give insight into methods of further violating Kasha's rule. Binding experiments of these dyes to protein, DNA or other biomolecules can be conducted to better understand molecular

torsion and/or substituent effects on fluorescence ratios and binding affinity. These could then be used for detection and/or destruction of unhealthy cells that have the unwanted characteristics that influence S_2/S_1 fluorescence ratio changes.

Beyond application, these findings expand our fundamental understanding of excited state dynamics in heptamethine cyanine dyes with the hope that these methods can be employed in other fluorophores.

BIBLIOGRAPHY

BIBLIOGRAPHY

(1) Kasha, M. Characterization of Electronic Transitions in Complex Molecules. *Discuss. Faraday Soc.* **1950**, *9* (c), 14–19.

(2) Sharafy, S.; Muszkat, K. A. Viscosity Dependence of Fluorescence Quantum Yields. **1968**, *12* (2), 4119–4125.

(3) Ebeid, E.-Z. M.; Abdel-Kader, M. H.; Issa, R. M.; El-Daly, S. A. Viscosity and Medium Effects on the Fluorescence and Photochemical Behaviour of Some Aryl Chalcones. *Chem. Phys. Lett.* **1988**, *146* (3–4), 331–336.

(4) El-Daly, S. A.; M-Ebeid, E.-Z.; Babaqi, A. S.; Al-Hazmy, S. M. Effect of Viscosity and Temperature on Some Photophysical Parameters of 9-Phenyl-10-Methoxy Anthracene. *J. Photochem. Photobiol. A Chem.* **2004**, *163* (3), 497–501.

(5) Doja, M. Q. The Cyanine Dyes. *Chem. Rev.* **1932**, *11* (3), 273–321.

(6) Mahmoud, A. M.; Morrow, J. P.; Pizzi, D.; Azizah, A. M.; Davis, T. P.; Tabor, R. F.; Kempe, K. Tuning Cellular Interactions of Carboxylic Acid-Side-Chain-Containing Polyacrylates: The Role of Cyanine Dye Label and Side-Chain Type. *Biomacromolecules* **2020**, *21* (8), 3007–3016.

(7) Guo, L.; Li, C.; Shang, H.; Zhang, R.; Li, X.; Lu, Q.; Cheng, X.; Liu, Z.; Sun, J. Z.; Yu, X. A Side-Chain Engineering Strategy for Constructing Fluorescent Dyes with Direct and Ultrafast Self-Delivery to Living Cells. *Chem. Sci.* **2020**, *11* (3), 661–670.

(8) Zhang, J.; Moemeni, M.; Yang, C.; Liang, F.; Peng, W.-T.; Levine, B. G.; Lunt, R. R.; Borhan, B. General Strategy for Tuning the Stokes Shifts of near Infrared Cyanine Dyes. *J. Mater. Chem. C* **2020**, *8* (47), 16769–16773.

(9) Urbanska, K.; Romanowska-Dixon, B.; Matuszak, Z.; Oszajca, J.; Nowak-Sliwinska, P.; Stochel, G. Indocyanine Green as a Prospective Sensitizer for Photodynamic. **2002**, *49* (2), 387–391.

(10) Shi, C.; Wu, J. B.; Pan, D. Review on Near-Infrared Heptamethine Cyanine Dyes as Theranostic Agents for Tumor Imaging, Targeting, and Photodynamic Therapy. *J. Biomed. Opt.* **2016**, *21* (5), 050901.

(11) Schaafsma, B. E.; Mieog, J. S. D.; Hutteman, M.; Van Der Vorst, J. R.; Kuppen, P. J. K.; Löwik, C. W. G. M.; Frangioni, J. V.; Van De Velde, C. J. H.; Vahrmeijer, A. L. The Clinical Use of Indocyanine Green as a Near-Infrared Fluorescent Contrast Agent for Image-Guided Oncologic Surgery. *J. Surg. Oncol.* **2011**, *104* (3), 323–332.

(12) Xu, B.; Gunn, J. M.; Dela Cruz, J. M.; Lozovoy, V. V.; Dantus, M. Quantitative Investigation of the Multiphoton Intrapulse Interference Phase Scan Method for Simultaneous Phase Measurement and Compensation of Femtosecond Laser Pulses. *J. Opt. Soc. Am. B* **2006**, *23* (4), 750.

(13) Coello, Y.; Lozovoy, V. V.; Gunaratne, T. C.; Xu, B.; Borukhovich, I.; Tseng, C.; Weinacht, T.; Dantus, M. Interference without an Interferometer: A Different Approach to Measuring, Compressing, and Shaping Ultrashort Laser Pulses. *J. Opt. Soc. Am. B* **2008**, *25* (6), A140.

(14) Lozovoy, V. V.; Rasskazov, G.; Pestov, D.; Dantus, M. Quantifying Noise in Ultrafast Laser Sources and Its Effect on Nonlinear Applications. *Opt. Express* **2015**, *23* (9), 12037.

(15) Laboe, M.; Lahiri, J.; Mohan T. M., N.; Liang, F.; Levine, B. G.; Beck, W. F.; Dantus, M. Linear and Nonlinear Optical Processes Controlling S2 and S1 Dual Fluorescence in Cyanine Dyes. *J. Phys. Chem. A* (**Submitted June 30, 2021**).

(16) Ballou, B.; Ernst, L. A.; Waggoner, A. S. Fluorescence Imaging of Tumors In Vivo. *Curr. Med. Chem.* **2005**, *12* (7), 795–805.

(17) Huang, B.; Jones, S. A.; Brandenburg, B.; Zhuang, X. Whole-Cell 3D STORM Reveals Interactions between Cellular Structures with Nanometer-Scale Resolution. *Nat. Methods* **2008**, *5* (12), 1047–1052.

(18) Pansare, V. J.; Hejazi, S.; Faenza, W. J.; Prud'homme, R. K. Review of Long-Wavelength Optical and NIR Imaging Materials: Contrast Agents, Fluorophores, and Multifunctional Nano Carriers. *Chem. Mater.* **2012**, *24* (5), 812–827.

(19) Zhang, Z.; Berezin, M. Y.; Kao, J. L. F.; d'Avignon, A.; Bai, M.; Achilefu, S. Near-Infrared Dichromic Fluorescent Carbocyanine Molecules. *Angew. Chemie - Int. Ed.* **2008**, *47* (19), 3584–3587.

(20) D.-H.; Schreiber, C. L.; Smith, B. D. Sterically Shielded Heptamethine Cyanine Dyes for Bioconjugation and High Performance Near-Infrared Fluorescence Imaging. *Angew. Chem. Int. Ed. Engl.* **2020**, *59* (29), 12154–12161.

(21) Sayama, K.; Tsukagoshi, S.; Mori, T.; Hara, K.; Ohga, Y.; Shinpou, A.; Abe, Y.; Suga, S.; Arakawa, H. Efficient Sensitization of Nanocrystalline TiO2 Films with Cyanine and Merocyanine Organic Dyes. *Sol. Energy Mater. Sol. Cells* **2003**, *80* (1), 47–71.

(22) Zhao, Y.; Meek, G. A.; Levine, B. G.; Lunt, R. R. Near-Infrared Harvesting Transparent Luminescent Solar Concentrators. *Adv. Opt. Mater.* **2014**, *2* (7), 606–611.

(23) Delaey, E.; van Laar, F.; De Vos, D.; Kamuhabwa, A.; Jacobs, P.; de Witte, P. A Comparative Study of the Photosensitizing Characteristics of Some Cyanine Dyes. *J. Photochem. Photobiol. B Biol.* **2000**, *55* (1), 27–36.

(24) Conceição, D. S.; Ferreira, D. P.; Vieira Ferreira, L. F. Photochemistry and Cytotoxicity Evaluation of Heptamethinecyanine near Infrared (NIR) Dyes. *Int. J. Mol. Sci.* **2013**, *14* (9), 18557–18571.

(25) Shindy, H.A. Fundamentals in the Chemistry of Cyanine Dyes: A Review. *Dye. Pigment.* **2017**, *145*, 505–513.

(26) Bricks, J. L.; Kachkovskii, A. D.; Slominskii, Y. L.; Gerasov, A. O.; Popov, S. V. Molecular Design of near Infrared Polymethine Dyes: A Review. *Dye. Pigment.* **2015**, *121*, 238–255.

(27) Bardeen, C. J.; Yakovlev, V. V.; Squier, J. A.; Wilson, K. R. Quantum Control of Population Transfer in Green Fluorescent Protein by Using Chirped Femtosecond Pulses. *J. Am. Chem. Soc.* **1998**, *120* (50), 13023–13027.

(28) Yakovlev, V. V.; Bardeen, C. J.; Che, J.; Cao, J.; Wilson, K. R. Chirped Pulse Enhancement of Multiphoton Absorption in Molecular Iodine. *J. Chem. Phys.* **1998**, *108* (6), 2309–2313.

(29) Mishima, K.; Hayashi, M.; Lin, J. T.; Yamashita, K.; Lin, S. H. A Numerical Study on Vibronic and Vibrational Dynamics Generated by Chirped Laser Pulses in the Presence of Relaxation Processes. *Chem. Phys. Lett.* **1999**, *309* (3–4), 279–286.

(30) Fainberg, B. D.; Narbaev, V. Chirped Pulse Excitation in Condensed Phases Involving Intramolecular Modes Studied by Double-Sided Feynman Diagrams for Fast Optical Dephasing. *J. Chem. Phys.* **2000**, *113* (18), 8113–8124.

(31) Misawa, K.; Kobayashi, T. Wave-Packet Dynamics in a Cyanine Dye Molecule Excited with Femtosecond Chirped Pulses. *J. Chem. Phys.* **2000**, *113* (17), 7546–7553.

(32) Konar, A.; Lozovoy, V. V.; Dantus, M. Solvent Environment Revealed by Positively Chirped Pulses. *J. Phys. Chem. Lett.* **2014**, *5*, 924–928.

(33) Nairat, M.; Webb, M.; Esch, M. P.; Lozovoy, V. V.; Levine, B. G.; Dantus, M. Time-Resolved Signatures across the Intramolecular Response in Substituted Cyanine Dyes. *Phys. Chem. Chem. Phys.* **2017**, *19* (21), 14085–14095.

(34) Nairat, M.; Konar, A.; Lozovoy, V. V.; Beck, W. F.; Blanchard, G. J.; Dantus, M. Controlling S2 Population in Cyanine Dyes Using Shaped Femtosecond Pulses. *J Phys Chem A.* **2016**, *120* (11), 1876–1885.

(35) Sharafy, S.; Muszkat, K. A. Viscosity Dependence of Fluorescence Quantum Yields. **1971**, *93* (17), 4119–4125.

(36) Loutfy, R. O.; Arnold, B. A. Torsional Relaxation of Molecular Rotors. **1982**, *1627* (1980), 4205–4211.

(37) Guarin, C. A.; Villabona-Monsalve, J. P.; López-Arteaga, R.; Peon, J. Dynamics of the Higher Lying Excited States of Cyanine Dyes. An Ultrafast Fluorescence Study. *J. Phys. Chem. B* **2013**, *117* (24), 7352–7362.

(38) Birks, J. B.; Dyson, D. J. The Relations Between the Fluorescence and Absorption Properties of Organic Molecules. *Proc. R. Soc. London, Ser. A* **1963**, *275* (1360), 135–148.

(39) Angulo, G.; Grampp, G.; Rosspeintner, A. Recalling the Appropriate Representation of Electronic Spectra. *Spectrochim. Acta A* **2006**, *65* (3–4), 727–731.

(40) Adamo, C.; Jacquemin, D. The Calculations of Excited-State Properties with Time-Dependent Density Functional Theory. *Chem. Soc. Rev.* **2013**, *42* (3), 845–856.

(41) Le Guennic, B.; Jacquemin, D. Taking Up the Cyanine Challenge with Quantum Tools. *Acc. Chem. Res.* **2015**, *48* (3), 530–537.

(42) Isborn, C. M.; Luehr, N.; Ufimtsev, I. S.; Martínez, T. J. Excited-State Electronic Structure with Configuration Interaction Singles and Tamm-Dancoff Time-Dependent Density Functional Theory on Graphical Processing Units. *J. Chem. Theory Comput.* **2011**, *7* (6), 1814–1823.

(43) Seritan, S.; Bannwarth, C.; Fales, B. S.; Hohenstein, E. G.; Isborn, C. M.; Kokkila-Schumacher, S. I. L.; Li, X.; Liu, F.; Luehr, N.; Snyder, J. W.; Song, C.; Titov, A. V.; Ufimtsev, I. S.; Wang, L. P.; Martínez, T. J. TeraChem: A Graphical Processing Unit-Accelerated Electronic Structure Package for Large-Scale Ab Initio Molecular Dynamics. *Wiley Interdiscip. Rev. Comput. Mol. Sci.* **2021**, *11* (2), 1–16.

(44) Ufimtsev, I. S.; Martinez, T. J. Quantum Chemistry on Graphical Processing Units. 3. Analytical Energy Gradients, Geometry Optimization, and First Principles Molecular Dynamics. *J. Chem. Theory Comput.* **2009**, *5* (10), 2619–2628.

(45) Yanai, T.; Tew, D. P.; Handy, N. C. A New Hybrid Exchange-Correlation Functional Using the Coulomb-Attenuating Method (CAM-B3LYP). *Chem. Phys. Lett.* **2004**, *393* (1–3), 51–57.

(46) Barone, V.; Cossi, M. Conductor Solvent Model. *J. Phys. Chem. A* **1998**, *102* (97), 1995–2001.

(47) Lange, A. W.; Herbert, J. M. A Smooth, Nonsingular, and Faithful Discretization Scheme for Polarizable Continuum Models: The Switching/Gaussian Approach. *J. Chem. Phys.* **2010**, *133* (24), 1–18.